Journal of Sound and Vibration (2002) **253**(4), 859–888
doi:10.1006/jsvi.2001.4072, available online at http://www.idealibrary.com on IDEAL®

BIFURCATIONS AND CHAOS OF AN IMMERSED CANTILEVER BEAM IN A FLUID AND CARRYING AN INTERMEDIATE MASS

A. A. Al-Qaisia

Department of Mechanical Engineering, Faculty of Engineering and Technology, University of Jordan, Amman 11942, *Jordan. E-mail: alqaisia@ju.edu.jo*

AND

M. N. Hamdan

Department of Mechanical Engineering, King Fahd University of Petroleum and Minerals, Dhahran, Saudi Arabia

(*Received* 18 *April* 2001, *and in final form* 10 *September* 2001)

The concern of this work is the local stability and period-doubling bifurcations of the response to a transverse harmonic excitation of a slender cantilever beam partially immersed in a fluid and carrying an intermediate lumped mass. The unimodal form of the non-linear dynamic model describing the beam–mass in-plane large-amplitude flexural vibration, which accounts for axial inertia, non-linear curvature and inextensibility condition, developed in Al-Qaisia *et al.* (2000 *Shock and Vibration* **7**, 179–194), is analyzed and studied for the resonance responses of the first three modes of vibration, using two-term harmonic balance method. Then a consistent second order stability analysis of the associated linearized variational equation is carried out using approximate methods to predict the zones of symmetry breaking leading to period-doubling bifurcation and chaos on the resonance response curves. The results of the present work are verified for selected physical system parameters by numerical simulations using methods of the qualitative theory, and good agreement was obtained between the analytical and numerical results. Also, analytical prediction of the period-doubling bifurcation and chaos boundaries obtained using a period-doubling bifurcation criterion proposed in Al-Qaisia and Hamdan (2001 *Journal of Sound and Vibration* **244**, 453–479) are compared with those of computer simulations. In addition, results of the effect of fluid density, fluid depth, mass ratio, mass position and damping on the period-doubling bifurcation diagrams are studies and presented.

1. INTRODUCTION

Offshore structures such as piles, oil platform supports, oil-loading terminals and towers surrounded by water are usually modelled as a beam or a column when studying its static or dynamic behavior. Since these structures are relatively flexible due to their high aspect ratio and because they are usually subjected to various excitation loads such as wind loads and wave loads, the prediction of their steady state responses and their stabilities, under various combinations of parameters, is greatly needed for design and analysis purposes.

0022-460X/02/$35.00

An understanding of the dynamic characteristic of a structural system is essential for its design and control. Many of the important characteristics can only be modelled by non-linear governing equations. Non-linearities can have important influences even when the amplitudes of the response are quite small, and certain responses may result, such as period-doubling bifurcation and chaos [1].

The route to chaos from regular period motion (or from chaos to regular periodic motion) through a sequence of period-doubling bifurcations in non-linear oscillators with single equilibrium positions has been the subject of many analytical and numerical investigations, see, e.g., references [2–11]. These studies and others have shown that this route to (or from) chaos can be adequately described by making use of approximate analytical methods to study various instabilities of approximate periodic solutions along with a computer simulation using methods of the qualitative theory. By making use of variational Hill-type equations to examine various instabilities of corresponding approximate periodic solutions, these studies have shown that it is possible to determine and describe with fair accuracy, if any, the zones of period-doubling bifurcations on the resonance curves of individual harmonic solutions. Then methods of qualitative theory with the aid of digital computer simulations were used in these studies to determine the locations of chaotic motion zones, which are preceded by period-doubling bifurcations. A literature review for different types of oscillators, regarding the behavior, i.e. period-doubling bifurcation, chaos and transition to chaos from regular periodic motion (or from chaos to regular periodic motion) [2–19] is discussed in detail in reference [20].

In the present work, the main concern is the approximate analysis, aided with computer simulations, of the stability, symmetry breaking and period-doubling bifurcation leading to chaos of approximate harmonic solutions of the harmonically driven non-linear oscillator having single equilibrium position and described by the general non-dimensional form [21]

$$\ddot{u} + \delta\dot{u} + u + \varepsilon_1 (u^2\ddot{u} + u\dot{u}^2) + \varepsilon_2 u^3 = P\cos(\Omega t). \tag{1}$$

The non-linear oscillator in equation (1) describes the unimodal in-plane flexural vibration response of a cantilever slender beam partially immersed in a fluid and carrying a point mass at an intermediate position along its span (see Figure 1). The derivation of this equation, described in detail in reference [21] and summarized in Appendix A for convenience, ignores the rotary inertia and shear deformation, but takes into account axial inertia and non-linear curvature.

The beam considered is assumed to be slender, i.e., similar to that considered by Zavodney and Nayfeh [22], Crespo da Silva and Glynn [23], Hamdan and Shabaneh [24], Al-Qaisia *et al.* [21] and Arafat *et al.* [25]. Such a slender beam system may undergo large bending motion without a significant axial deformation and therefore is assumed to be extensible. In addition, the natural frequencies of the axial motion are much higher than those of the bending motion. The beam–mass system is subjected to a transverse harmonic excitation load at an intermediate point along its span. Furthermore, following reference [26], the model in equation (1) assumes that the effect of the fluid–structure interaction can be taken as an added inertia to the structure.

The present physical problem model, equation (1), belongs to the general class of oscillators studied in reference [20] and presents a physical example of such oscillators. The interest of the present study is to present the effect of various system physical parameters; effect of fluid density, fluid depth, mass ratio, mass position and damping on the system period-doubling bifurcation. In equation (1) u represents a dimensionless beam tip displacement, δ the damping of the system and the parameters ε_1, ε_2 and P (see Appendix A) are dimensionless constants which depend on the beam–mass system physical

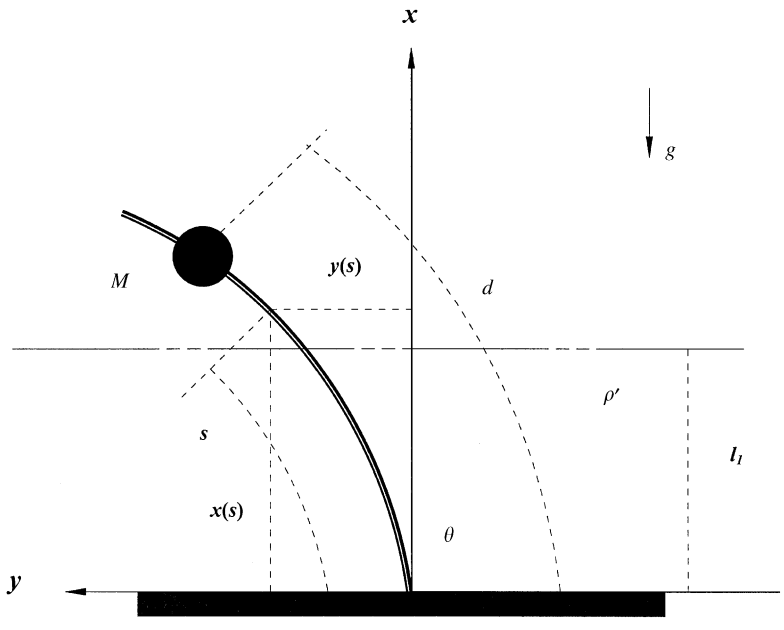

Figure 1. A schematic of the immersed cantilever beam under consideration.

TABLE 1

Values of the parameters in the temporal equation (1) *of the beam system shown in Figure* 1 *with the physical characteristics*; *attached mass magnitude ratio* $\mu = 0{\cdot}25$, *relative position* $\eta = 0{\cdot}75$, *relative position of the applied concentrated load* $\zeta_c = 0{\cdot}7$ *and relative depth* $\zeta_1 = 0{\cdot}5$ *of the immersed part*, *calculated from equations* (A17–A21, A25) *for the first four modes of vibration*

	Mode			
	1	2	3	4
p	1·875104	4·694091	7·854757	10·99554
α_1	1·450759848	1·175825329	1·519188317	1·565111561
α_2	12·32839815	485·3450482	3806·040655	14616·18988
α_3	5·330115538	149·9670172	1027·160859	4123·530484
α_4	20·22032802	6709·048744	132182·7099	964052·2595
α_5	1·181752528	0·634103731	− 1·314851876	0·794780663
ε_1	1·044937644	5·788285351	10·95875813	21·79168359
ε_2	0·932955265	1·254692582	1·125811592	1·091096770
ε_3	0·179740211	0·006132834	− 0·002713539	0·000597900

characteristics, forcing magnitude and location and the considered mode; examples of the calculated numerical values of these parameters for selected beam system physical parameters are shown in Table 1. The objects of interest here are the cases where the oscillator in equation (1) is not weakly non-linear, i.e., when the displacement u is of order unity, ε_1 and/or ε_2 are not necessarily small compared to unity. In the above oscillator, which has a single equilibrium position at $u = 0$, the two non-linear terms inside the

parentheses are of inertial type having a net softening effect, while the last non-linear term is of the hardening type. Thus, depending on the relative values of ε_1 and ε_2, these characteristics of frequency resonance response curves of this oscillator may be of softening or hardening type. These characteristics were studied in reference [27] using the harmonic balance method (HB) and the second order perturbation multiple-time scale (MMS) with reconstitution versions I and II. The results in references [21, 27] show that the two modes harmonic balance method yields quantitatively fairly accurate and qualitatively accurate solutions even when the oscillator is relatively strongly non-linear. Approximations to the resonance response, symmetric and asymmetric and their stabilities and analytical prediction of period-doubling bifurcation and chaos boundaries using the period-doubling bifurcation criterion proposed in reference [20] and compared with the computer simulations, of the non-linear oscillator, described in equation (1), are presented and discussed in the following sections, for the first, second and third natural frequencies, which may take place when the forcing frequency is arbitrarily varied to be close to one of these system natural frequencies.

2. APPROXIMATE SYMMETRIC HARMONIC BALANCE SOLUTIONS

An approximate solution to the oscillator in equation (1) may be obtained by using the harmonic balance method which does not place a restriction on the order of magnitude of non-linear terms relative to linear ones, i.e., ε_1 and ε_2 need not be small compared to 1 [21, 27]. For convenience, equation (1) is rewritten in terms of a new time scale $T = \Omega t$, so that it becomes

$$\Omega^2\ddot{u} + \Omega\delta\dot{u} + u + \varepsilon_1\Omega^2u^2\ddot{u} + \varepsilon_1\Omega^2u\dot{u}^2 + \varepsilon_2u^3 = P\cos(T + \phi), \tag{2}$$

where dots now denote derivatives with respect to the new time T, and the unknown constant phase ϕ has been added to the harmonic excitation so that one can obtain a harmonic balance solution in which the fundamental has a cosine term only. A two-term approximate symmetric solution to equation (2) can be obtained by substituting

$$u(T) = A_1\cos T + A_3\cos 3T + B_3\sin 3T \tag{3}$$

into equation (2), where A_1, A_3, B_3 and ϕ can be determined by the harmonic balance method (HB), and solving the set of non-linear algebraic equations for A_1, A_3, B_3 and ϕ. Results for the steady state response using the two-term harmonic balance method (2THB) were presented in references [21, 27] for different values of the parameters δ, ε_1, ε_2 and P, which are the physical parameters of the first three modes of vibration of the immersed cantilever beam system shown in Figure 1. For convenience, the relations defining steady state resonance response of equation (2) obtained by applying the harmonic balance method using single term (SHB) and two terms (2THB) are, for convenience, presented in Appendix B.

3. STABILITY ANALYSIS OF SYMMETRIC HARMONIC BALANCE SOLUTIONS

The stability analysis of the approximate harmonic balance solution in equation (3) may be carried out by introducing a small perturbation $v(T)$ to the assumed solution (3), i.e., by substituting

$$u(T) = A_1\cos T + A_3\cos 3T + B_3\sin 3T + v(T) \tag{4}$$

into equation (2). This leads to the following linearized variational equation:

$$\begin{aligned}
&\ddot{v}\Omega^2 \Big\{1 + \frac{\varepsilon_1}{2}(A_1^2 + A_3^2 + B_3^2 + (A_1^2 + 2A_1A_3)\cos 2T + 2A_1A_3\cos 4T \\
&\quad + (A_3^2 + B_3^2)\cos(6T + 2A_1B_3(\sin 2T + \sin 4T) + 2A_3B_3\sin 6T)\Big\} \\
&\quad + \dot{v}\{\delta\Omega + \varepsilon_1\Omega^2(2A_1B_3\cos 2T + 4A_1B_3\cos 4T + 6A_3B_3\cos 6T \\
&\quad - (A_1^2 + 2A_1A_3)\sin 2T - 4A_1A_3\sin 4T + 3(B_3^2 - A_3^2)\sin 6T)\} \\
&\quad + v\Big\{1 + \frac{3}{2}\varepsilon_2(A_1^2 + A_3^2 + B_3^2) - \frac{\varepsilon_1}{2}\Omega^2(A_1^2 + 9A_3^2 + 9B_3^2) \\
&\quad + (\tfrac{3}{2}\varepsilon_2 A_1^2 + 3\varepsilon_2A_1A_3 - \tfrac{3}{2}\varepsilon_1\Omega^2A_1^2 - 7\varepsilon_1\Omega^2A_1A_3)\cos 2T \\
&\quad + (3\varepsilon_2A_1A_3 - 13\varepsilon_1\Omega^2A_1A_3)\cos 4T \\
&\quad + (\tfrac{1}{2}(3\varepsilon_2(A_3^2 - B_3^2) - 27\varepsilon_1\Omega^2(A_3^2 + B_3^2)))\cos 6T \\
&\quad + (3\varepsilon_1A_1B_3 - 7\varepsilon_1\Omega^2A_1B_3)\sin 2T + (3\varepsilon_2A_1B_3 - 13\varepsilon_1\Omega^2A_1B_3)\sin 4T \\
&\quad + (3\varepsilon_2A_3B_3 - 27\varepsilon_1\Omega^2A_3B_3)\sin 6T\Big\} = 0. \qquad (5)
\end{aligned}$$

Then by virtue of the Floquet theory, a particular solution of the linearized variational equation (LVE), is sought in the form [2]

$$v(T) = \mathrm{e}^{\beta T}\eta(T), \qquad (6)$$

where β is defined as the characteristic exponent and $\eta(T)$ is a periodic function with periods T and $T/2$. The solution of $v(T)$ is stable (respectively, unstable) if the real part of β is negative (positive); and the real part of β is zero on the boundary between stable and unstable regions [11].

The approximate theory of the Hill-type equations allows one to assume functions $\eta_{\mathrm{I}}(T)$ and $\eta_{\mathrm{II}}(T)$ as truncated Fourier series, so that at the stability boundaries, i.e., $\beta = 0$, the disturbances are sought as

$$\eta_{\mathrm{I}}(T) = v(T)_{\beta=0} = \sum_m^{\infty} b_m\cos(mT + \psi_m) = b_{mc}\cos(mT) + b_{ms}\sin(mT),\ m = 1, 3, 5 \ldots \infty, \qquad (7)$$

$$\eta_{\mathrm{II}}(T) = v(T)_{\beta=0} = b_0 + \sum_m^{\infty} b_m\cos(mT + \psi_m) = b_0 + b_{mc}\cos(mT) + b_{ms}\sin(mT),\ m = 2, 4, 6 \ldots \infty. \qquad (8)$$

The instabilities of type I (first order stability) ,are those which bring odd harmonic components to the system response, while type II (second order stability) gives a build-up of the even harmonic component [2, 20], which is the interest of the present work, i.e., stability boundaries at which the possibility of period-doubling bifurcation (PDB) and chaos may occur.

The first and second order unstable regions can be predicted by substituting equations (7) and (8) into the linearized variational equation (LVE) (5) and using the harmonic balance method. This leads to an infinite set of linear homogeneous equations (b_{mc} and b_{ms}, $m = 1, 3, 5 \ldots \infty$ for analysis I or b_0, b_{mc} and b_{ms}, $m = 2, 4, 6 \ldots \infty$ for analysis II). These equations can be expressed in the matrix from as $\mathbf{Mb} = \mathbf{0}$, where $\mathbf{b}$ is one of the two column vectors $(\ldots, b_{ic}, b_{is}, \ldots)^{\mathrm{T}}$, and $(b_0, \ldots, b_{ic}, b_{is}, \ldots)^{\mathrm{T}}$; $\mathbf{M}$ is the characteristic matrix. Non-trivial solutions for b_m exist only when the determinant (Δ) of the characteristic matrix vanishes. This determinant depends on β, thus $\Delta(\beta) = 0$ provides the characteristic equation for β. The stability conditions become $\Delta(\beta = 0)$ is positive (respectively, negative) is a stable (unstable) region, and $\Delta(\beta = 0) = 0$ at the boundary between the stable and unstable regions [11].

To determine the boundaries of the second unstable region "i.e., analysis II" according to the above procedure, one may substitute as a first approximation

$$v(T) = b_0 + b_{2c}\cos 2T + b_{2s}\sin 2T + b_{4c}\cos 4T + b_{4s}\sin 4T \tag{9}$$

into the LVE (5), and upon applying the harmonic balance this leads to a set of linear homogeneous equations for b_0, b_{2c}, b_{2s}, b_{4c} and b_{4s}, that can be written in a matrix form as

$$\mathbf{Mb} = \mathbf{0} \tag{10}$$

where $\mathbf{b}$ is the column vector $(b_0, b_{2c}, b_{2s}, b_{4c}, b_{4s})^{\mathrm{T}}$ and $\mathbf{M}$ is the characteristic matrix. The elements of the coefficient matrix $\mathbf{M}$ are

$$M_{11} = 1 + \tfrac{3}{2}\varepsilon_2 (A_1^2 + A_3^2 + B_3^2) - \tfrac{1}{2}\varepsilon_1 \Omega^2 (A_1^2 + 9A_3^2 + 9B_3^2),$$

$$M_{12} = \tfrac{1}{2} A_1 B_3 (3\varepsilon_2 - 7\varepsilon_1 \Omega^2),$$

$$M_{13} = \tfrac{3}{4}\varepsilon_2 (A_1^2 + 6A_1 A_3) - \tfrac{1}{4}\varepsilon_1 \Omega^2 (3A_1^2 + 17A_1 A_3),$$

$$M_{14} = \tfrac{1}{2} A_1 B_3 (3\varepsilon_2 - 13\varepsilon_1 \Omega^2), \qquad M_{15} = \tfrac{1}{2} A_1 A_3 (3\varepsilon_2 - 13\varepsilon_1 \Omega^2),$$

$$M_{21} = \frac{\varepsilon_2}{2}(3A_1^2 + 6A_1 A_3) - \tfrac{1}{2}\varepsilon_1 \Omega^2 (3A_1^2 + 14A_1 A_3),$$

$$M_{22} = 2\Omega\delta + \tfrac{1}{2} A_1 B_3 (3\varepsilon_2 - 9\varepsilon_1 \Omega^2),$$

$$M_{23} = 1 - 4\Omega^2 + \tfrac{1}{2}\varepsilon_2 (A_1^2 + A_1 A_3 + A_3^2 + B_3^2) - \tfrac{1}{2}\varepsilon_1 \Omega^2 (5A_1^2 + 9A_1 A_3 + 13A_3^2 + 13B_3^2),$$

$$M_{24} = \tfrac{1}{2} B_3 (3\varepsilon_2 (A_1 + A_3) - \varepsilon_1 \Omega^2 (15A_1 + 19A_3)),$$

$$M_{25} = \tfrac{1}{4}\varepsilon_2 (3A_1^2 + 6A_1 A_3 + 3A_3^2 - 3B_3^2) - \tfrac{1}{4}\varepsilon_1 \Omega^2 (11A_1^2 + 30A_1 A_3 + 19A_3^2 + 19B_3^2),$$

$$M_{31} = A_1 B_3 (3\varepsilon_2 - 7\varepsilon_1 \Omega^2),$$

$$M_{32} = 1 - 4\Omega^2 + \tfrac{3}{2}\varepsilon_2 (A_1^2 - A_1 A_3 + A_3^2 + B_3^2) - \tfrac{1}{2}\varepsilon_1 \Omega^2 (5A_1^2 - 9A_1 A_3 + 13A_3^2 + 13B_3^2),$$

$$M_{33} = \tfrac{1}{2}A_1B_3\,(3\varepsilon_2 - 9\varepsilon_1\Omega^2) - 2\Omega\delta,$$

$$M_{34} = \tfrac{1}{4}\varepsilon_2(3A_1^2 + 6A_1A_3 - 3A_3^2 + 3B_3^2) - \tfrac{1}{4}\varepsilon_1\Omega^2\,(11A_1^2 + 15A_1A_2 - 19A_3^2 + 19B_3^2),$$

$$M_{35} = \tfrac{1}{2}B_3\,(3\varepsilon_2\,(A_3 - A_1) + \varepsilon_1\Omega^2(15A_1 - 19A_3)),$$

$$M_{41} = A_1A_3\,(3\varepsilon_2 - 13\varepsilon_1\Omega^2),$$

$$M_{42} = \tfrac{1}{2}B_3(3\varepsilon_2(A_3 - A_1) + \varepsilon_1\Omega^2\,(15A_1 - 19A_3)),$$

$$M_{43} = \tfrac{1}{4}\varepsilon_2(3A_1^2 + 6A_1A_3 + 3A_3^2 - 3B_3^2) - \tfrac{1}{4}\varepsilon_1\Omega^2\,(11A_1^2 + 15A_1A_3 + 19A_3^2 - 19B_3^2),$$

$$M_{44} = 4\Omega\delta,$$

$$M_{45} = 1 - 16\Omega^2 + \tfrac{3}{2}\varepsilon_2(A_1^2 + A_3^2 + B_3^2) - \tfrac{1}{2}\varepsilon_1\Omega^2\,(17A_1^2 + 25A_3^2 + 25B_3^2),$$

$$M_{51} = A_1B_3\,(3\varepsilon_2 - 13\varepsilon_1\Omega^2),$$

$$M_{52} = \tfrac{1}{4}\varepsilon_2\,(3A_1^2 + 6A_1A_3 - 3A_3^2 + 3B_3^2) - \tfrac{1}{4}\varepsilon_1\Omega^2\,(11A_1^2 + 15A_1A_3 - 19A_3^2 + 19B_3^2),$$

$$M_{53} = \tfrac{1}{2}\,B_3\,(3\varepsilon_2\,(A_1 + A_3) - \varepsilon_1\Omega^2\,(15A_1 + 19A_3)),$$

$$M_{54} = 1 - 16\Omega^2 + \tfrac{3}{2}\varepsilon_2(A_1^2 + A_3^2 + B_3^2) - \tfrac{1}{2}\varepsilon_1\Omega^2\,(17A_1^2 + 25A_3^2 + 25B_3^2),$$

$$M_{55} = -\,4\Omega\delta.$$

Non-trivial solutions for b_0, b_{2c}, b_{2s}, b_{4c} and b_{4s} exist only when the determinant of the coefficient matrix $\mathbf{M}$ in equation (10) vanishes, which gives the second order stability boundaries that intersect with the steady state response curves of the nonlinear oscillator described in equation (2) obtained by using the two-term harmonic balance solution (3).

4. APPROXIMATE ASYMMETRIC SOLUTIONS AND THEIR STABILITIES

By using the harmonic balance method, an asymmetric periodic solution to equation (2) in the first approximation takes the form

$$u(T) = A_0 + A_1 \cos T, \tag{11}$$

where A_0 is a constant bias and A_1 is the amplitude. Substituting equation (11) and its derivatives into equation (2), one obtains

$$A_1\left[A_0^2(3\varepsilon_2 - \varepsilon_1\Omega^2) + \frac{A_1^2}{4}\,(3\varepsilon_2 - 2\varepsilon_1\Omega^2) + 1 - \Omega^2\right] = P\cos\phi, \tag{12}$$

$$A_1\delta\Omega = P\,\sin\,\phi, \qquad A_0\left[A_0^2\varepsilon_2 + \frac{A_1^2}{2}\,(3\varepsilon_2 - \varepsilon_1\Omega^2) + 1\right] = 0. \tag{13, 14}$$

For $A_0 \neq 0$, it follows from equation (14) that

$$A_0^2 = \frac{1}{\varepsilon_2}\left[\frac{A_1^2}{2}(\varepsilon_1\Omega^2 - 3\varepsilon_2) - 1\right]. \tag{15}$$

Equations (12), (13) and (15) yield (in terms of A_1 only) the frequency response equation of the system, using the biased solution (11):

$$\begin{aligned}
&\left(\tfrac{225}{16}\varepsilon_2^4 - \tfrac{75}{4}\varepsilon_1\varepsilon_2^3\Omega^2 + 10\varepsilon_1^2\varepsilon_2^2\Omega^2 - \tfrac{5}{2}\varepsilon_1^3\varepsilon_2\Omega^6 + \tfrac{1}{4}\varepsilon_1^4\Omega^8\right)A_1^6 \\
&\quad + \left(15\varepsilon_2^3 - \tfrac{35}{2}\varepsilon_1\varepsilon_2^2\Omega^2 + \tfrac{15}{2}\varepsilon_2^3\Omega^2 + 7\varepsilon_1^2\varepsilon_2\Omega^4 - 5\varepsilon_1\varepsilon_2^2\Omega^4 - \varepsilon_1^3\Omega^6 + \varepsilon_1^2\varepsilon_2\Omega^6\right)A_1^4 \\
&\quad + \left(4\varepsilon_2^2 + \delta^2\Omega^2 - 4\varepsilon_1\varepsilon_2\Omega^2 + 4\varepsilon_2^2\Omega^2 + \varepsilon_1^2\Omega^1 - 2\varepsilon_1\varepsilon_2\Omega^4 + \varepsilon_2^2\Omega^4\right)A_1^2 = P^2.
\end{aligned} \tag{16}$$

Steady state resonance curves A_0 and A_1 can be determined from equations (15) and (16) respectively.

The stability of the assumed solution (11), can be examined by using the same procedure followed in the previous section: i.e., by substituting $u(T) = A_0 + A_1\cos T + v(T)$ into equation (2). This yields the following linearized version of the variational equation:

$$\begin{aligned}
&\ddot{v}\Omega^2\left[1 + \frac{A_1^2}{2}\varepsilon_1(1+\cos 2T) + \varepsilon_1(A_0^2 + 2A_0A_1\cos 2T)\right] \\
&\quad + \dot{v}\left[\delta\Omega - \varepsilon_1\Omega^2(A_1^2\sin 2T + 2A_0A_1\sin T)\right] \\
&\quad + v\left[1 + \frac{A_1^2}{2}(3\varepsilon_2(1+\cos 2T) - \varepsilon_1\Omega^2(1+3\cos 2T)) + 3\varepsilon_2A_0^2 + 2A_0A_1\cos T(3\varepsilon_2 - \varepsilon_1\Omega^2)\right] = 0.
\end{aligned} \tag{17}$$

It is clear that equation (17) has two parametric excitations with periods T and $T/2$. To examine the period-doubling bifurcation in the first approximation of the biased solution, one may seek a particular solution at the stability limit as

$$v(T) = b_{1/2}\cos\left(\frac{T}{2} + \psi_{1/2}\right) = b_{1/2)c}\cos\left(\frac{T}{2}\right) + b_{1/2)s}\sin\left(\frac{T}{2}\right). \tag{18}$$

Then, by substituting equation (18) and its derivatives into equation (17), and applying the harmonic balance method, writing the set of linear homogeneous equations for $b_{1/2)c}$ and $b_{1/2)s}$ in a matrix form $\mathbf{Mb} = \mathbf{0}$ and putting the condition of non-trival solution for $b_{1/2)c}$ and $b_{1/2)s}$. The elements of the coefficient matrix are

$$\begin{aligned}
M_{11} &= 1 - \frac{\Omega^2}{4} + 3\varepsilon_2\left(A_0^2 - A_0A_1 + \frac{A_1^2}{2}\right) - \frac{\varepsilon_1\Omega^2}{8}(2A_0^2 - 6A_0A_1 + 5A_1^2), \\
M_{21} &= -\frac{\Omega\delta}{2}, \qquad M_{12} = \frac{\Omega\delta}{2}, \\
M_{22} &= 1 - \frac{\Omega^2}{4} + 3\varepsilon_2\left(A_0^2 + A_0A_1 + \frac{A_1^2}{2}\right) - \frac{\varepsilon_1\Omega^2}{8}(2A_0^2 + 6A_0A_1 + 5A_1^2).
\end{aligned} \tag{19}$$

A non-trivial solution for $b_{1/2)c}$, $b_{1/2)s}$ exists only when the determinant of the coefficient matrix **M** vanishes, which gives the unstable portions of the asymmetric solution of the non-linear oscillator obtained by using equations (15) and (16). A relation between the amplitudes (A_0 and A_1) and the frequency Ω to be satisfied at the stability boundary can be obtained from the determinant of the coefficient matrix **M**, such that

$$\Omega^4\left(\frac{1}{16}+\frac{\varepsilon_1}{16}(2A_0^2+5A_1^2)+\frac{\varepsilon_1^2}{64}(4A_0^4-16A_0^2A_1^2+25A_1^4)\right)$$
$$+\Omega^2\left(\frac{\delta^2}{4}-\frac{1}{2}-\frac{3\varepsilon_2}{4}(2A_0^2+A_1^2)-\frac{\varepsilon_1\varepsilon_2}{8}(12A_0^4+15A_1^4)-\frac{\varepsilon_1}{4}(2A_0^2+5A_1^2)\right)$$
$$+\left(1+3\varepsilon_2(2A_0^2+A_1^2)+9\varepsilon_2^2\left(A_0^4+\frac{A_1^2}{4}\right)\right)=0. \tag{20}$$

5. CRITERION FOR PERIOD-DOUBLING BIFURCATIONS

Period-doubling bifurcations in many non-linear systems occur just before the onset of chaos. Therefore, PDBs may be considered often the lower threshold of chaos [16]. A criterion that might predict the necessary physical system parameters combination for this type of non-linear oscillators which models the immersed beam–mass system shown in Figure 1, is presented and discussed in reference [20]. However, once the second unstable region intersects with the steady state response curve, i.e., equation (C10) is satisfied, one can use this equation which gives the critical bifurcation value of the amplitude as a function of the frequency and the system physical parameters, $A_{cr} \equiv A_{cr}(\Omega, \varepsilon_1, \varepsilon_2, \delta)$. Upon substituting the value of A_{cr} into the frequency response equation (B4), one can obtain the critical value of the forcing parameter [20], such that

$$(\tfrac{1}{16}(9\varepsilon_2^2-12\varepsilon_1\varepsilon_2\Omega^2+4\varepsilon_1^2\Omega^4))A_{cr}^6+(\tfrac{3}{2}\varepsilon_2(1-\Omega^2)+\varepsilon_1(\Omega^4-\Omega^2))A_{cr}^4$$
$$+(1+\Omega^2(\delta^2-2)+\Omega^4)A_{cr}^2=P_{cr}^2. \tag{21}$$

The results of computer simulations presented in reference [20] show that the above criterion gives a reasonable prediction of the minimum value of the forcing parameter required for period-doubling bifurcation and may be used as a threshold criterion for PDB.

6. ANALYTICAL RESULTS

The stability analysis of the non-linear oscillator, single mode, temporal equation of motion (1) of the immersed cantilever beam carrying an intermediate lumped mass 'Figure 1' was calculated and verified near the resonance response zone, for the first three modes of vibration and for selected values of system parameters P, δ and the corresponding ε_1 and ε_2 for each mode, by assuming that the forcing frequency Ω is arbitrarily varied to be close to one of the system natural frequencies, i.e., the first three natural frequencies of the beam–mass system. As an example, if the beam in Figure 1 is taken to be an aluminum beam, with density $\rho = 2800\,\text{kg/m}^3$, modulus of elasticity $E = 70\,\text{GPa}$, cross-sectional area $5\,\text{cm} \times 5\,\text{cm}$ and length $l = 2\,\text{m}$. The fluid is taken to be water $\rho' = 1000\,\text{kg/m}^3$, so that $K_m = 1/2{\cdot}8$. The added inertia coefficient was taken as in reference [26], $C_m = 1{\cdot}0$, and the

non-dimensional gravity parameter g_0 is calculated to be 0·015. The selected values of the attached mass magnitude ratio μ, relative position η, relative position of the applied concentrated load ζ_c and relative depth ζ_l of the immersed part used in this work were $\mu = 0{\cdot}25$, $\eta = 0{\cdot}75$, $\zeta_c = 0{\cdot}7$, and $\zeta_1 = 0{\cdot}5$ respectively. By using these values and evaluating the integrals in equations (A18–A21), the calculated values of ε_1 and ε_2 for the first, second and third modes were calculated to be ($\varepsilon_1 = 1{\cdot}0449$, $\varepsilon_2 = 0{\cdot}9329$), ($\varepsilon_1 = 5{\cdot}7882$, $\varepsilon_2 = 1{\cdot}2546$) and ($\varepsilon_1 = 10{\cdot}9587$, $\varepsilon_2 = 1{\cdot}1258$), respectively, which are the same values considered and studied in detail in reference [21] to obtain results for the resonance response and first order stability of the beam–mass system shown in Figure 1.

The response of the non-linear oscillator is controlled by two competing softening "$\varepsilon_1 (u^2\ddot{u} + u\dot{u}^2)$" and hardening "$\varepsilon_2 u^3$" non-linearities, which exhibit fundamentally two different response characteristics [21, 27], depending on the relative value of ε_1 and ε_2. From the calculated values of ε_1 and ε_2 for the beam–mass system considered, the first mode resonance response exhibits, as expected, a hardening behavior, due to the fact that $(\varepsilon_1/\varepsilon_2 \cong 1{\cdot}12) < 1{\cdot}6$, while the response of the second and the higher modes exhibit a softening behavior as the ratio $(\varepsilon_1/\varepsilon_2) > 1{\cdot}6$: i.e., the response is dominated by the inertia non-linearities [21, 24, 27].

In Figure 2, the resonance response curve of the first mode was obtained by using the HB method; first and second order unstable regions are obtained by using a single term only and the values of parameters P and δ were chosen to be 10 and 0·02 respectively. The same figure shows also the biased solution given in equation (11). From the results in Figure 2, the second unstable region intersects with the response curve in two regions: $0{\cdot}645 < \Omega < 0{\cdot}695$ and at $\Omega \geqslant 2{\cdot}45$, while the asymmetric solution intersects with the response curve at

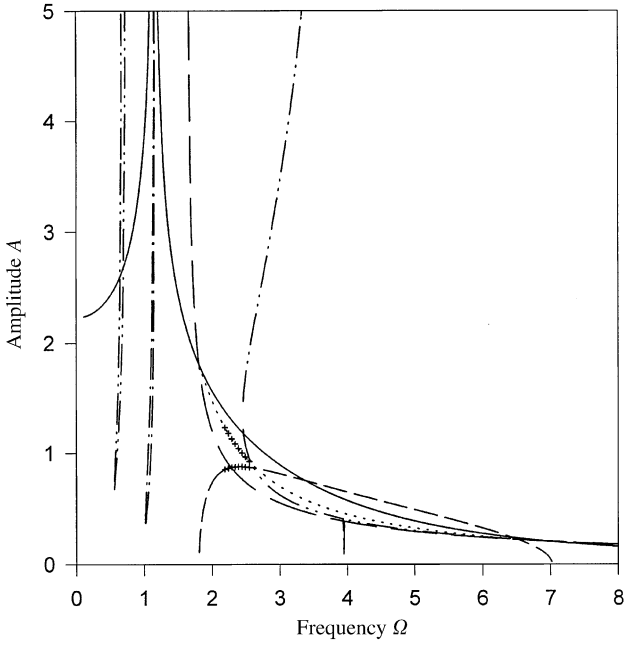

Figure 2. Steady state frequency response (SSFR), first order stability (1st Stab.), second order stability (2nd Stab.), biased solution and its stability using single term only for the first mode, i.e. $P = 10, \varepsilon_1 = 1{\cdot}0449, \varepsilon_2 = 0{\cdot}9329$ and $\delta = 0{\cdot}02$: ———, SSFR; – · – · –, 1st Stab.; — · —, 2nd Stab.; ····· A_0; – – – – –, A_1. + + + + + +, unstable A_0 and A_1; — — —, A_{+ve} "positive value of A in the symmetric solution at which A_0 in the biased solution has non-zero real value, calculated from equation (15)".

$\Omega > 1{\cdot}81$ and the unstable region for the asymmetric solution is between $2{\cdot}19 < \Omega < 2{\cdot}55$. To improve the accuracy of the predicted resonance response and stability, results were obtained and are shown in Figure 3 for the first mode, but with two terms used for the steady state response, i.e., equation (3), and stability analysis, i.e., using two terms in the assumed solution (4) of the linearized variational equation (5) to obtain results for the second order stability. As one may expect the predicted unstable regions of the response curve when using two terms are modified and they become $0{\cdot}683 < \Omega < 0{\cdot}719$ and $2{\cdot}2668 < \Omega < 6{\cdot}8965$.

In Figures 4 and 5 are shown the resonance response, first and second order unstable regions as obtained by using two terms for the second and third modes respectively. Also shown in the same figures are the biased solutions given by equation (11). From Figure 4, i.e., results for the second mode $P = 2{\cdot}5$, $\varepsilon_1 = 5{\cdot}7882$, $\varepsilon_2 = 1{\cdot}2546$, $\delta = 0{\cdot}02$, one can see that the predicted second unstable regions are $0{\cdot}393 < \Omega < 0{\cdot}4046$ and $1{\cdot}5043 < \Omega < 3{\cdot}4891$ and the asymmetric solution intersects with the response curve at $\Omega \geqslant 0{\cdot}95$ and the unstable region for the asymmetric solution is $1.20 < \Omega < 1{\cdot}83$. From Figure 5, i.e., results for the third mode $P = 3{\cdot}5$, $\varepsilon_1 = 10{\cdot}9587$, $\varepsilon_2 = 1{\cdot}1258$, $\delta = 0{\cdot}1$, one can see that the predicted second unstable regions are $0{\cdot}275 < \Omega < 0{\cdot}29$ and $1{\cdot}16 < \Omega < 5{\cdot}845$ and the asymmetric solution intersects with the resonance response curve at $\Omega \geqslant 0{\cdot}63$ and the unstable region for the asymmetric solution is $0.79 < \Omega < 1{\cdot}14$.

The effect of varying the physical parameters of the system, i.e., the attached mass magnitude ratio μ, relative position η, relative depth ζ_1 of the immersed part, fluid density parameter K_m and the damping δ, on the proposed criterion for PDB has been studied and is presented in Figures 6–10 for the second mode. It can be seen from Figures 6–8 that the value of the lower threshold force for PDB, i.e., equation (21), increases as the values of δ, ζ_1 and K_m increase, and this is due to the fact that as long as the relative depth ζ_1 of the

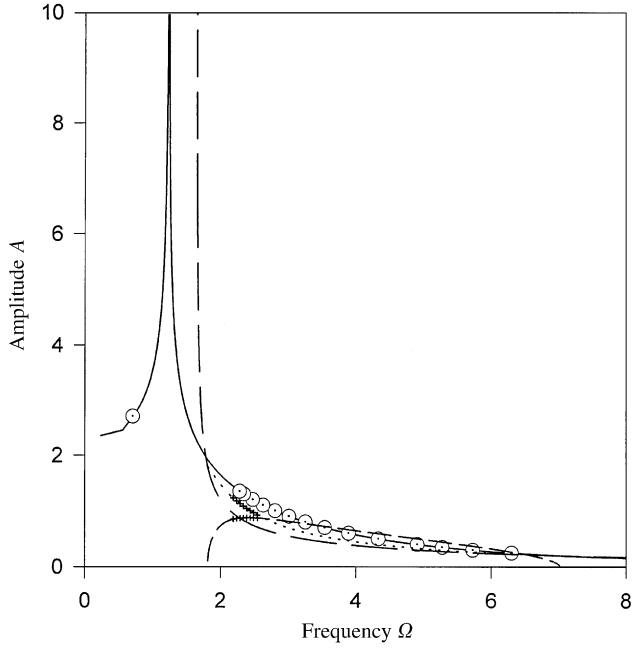

Figure 3. Steady state frequency response (SSFR), first order stability (1st Stab.), second order stability (2nd Stab.) as obtained by using two terms for the first mode. $P = 10$, $\varepsilon_1 = 1{\cdot}0449$, $\varepsilon_2 = 0{\cdot}9329$ and $\delta = 0{\cdot}02$: ————, SSFR "A_1 of equation (3)"; ○, 2nd Stab.; ●, 1st Stab. A_0, A_1, $A_{+\text{ve}}$ same as in Figure 2.

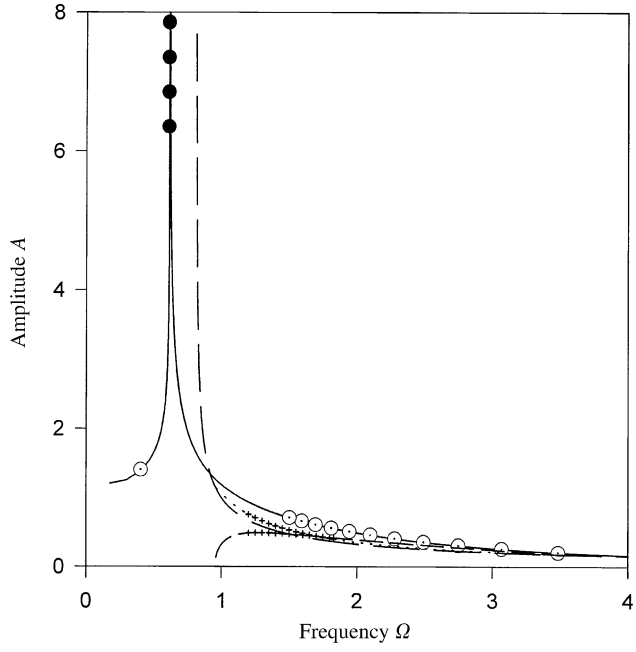

Figure 4. Same as in Figure 3, but for the second mode: i.e., $P = 2{\cdot}5$, $\varepsilon_1 = 5{\cdot}7882$, $\varepsilon_2 = 1{\cdot}2546$ and $\delta = 0{\cdot}02$.

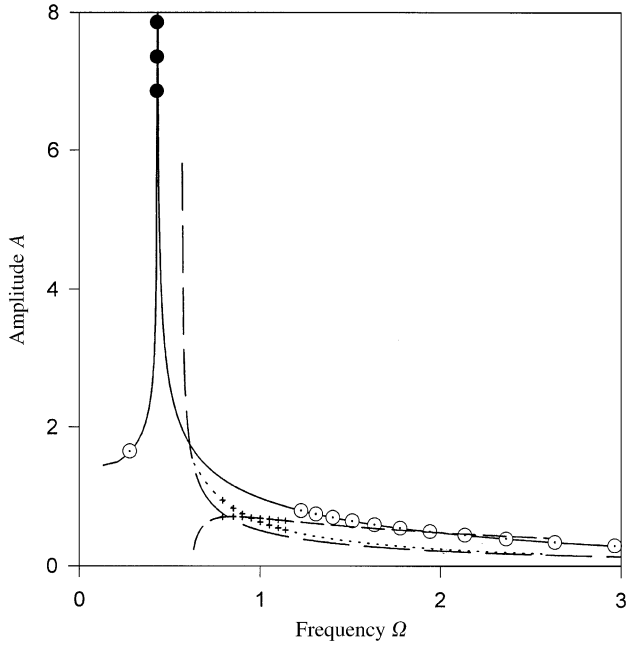

Figure 5. Same as in Figure 3, but for the third mode: i.e., $P = 3{\cdot}5$, $\varepsilon_1 = 10{\cdot}9587$, $\varepsilon_2 = 1{\cdot}1258$ and $\delta = 0{\cdot}1$.

immersed beam, the damping δ and fluid density parameter K_m increase, the force level required to oscillate the system will increase and as a result the lower threshold force for PDB will increase.

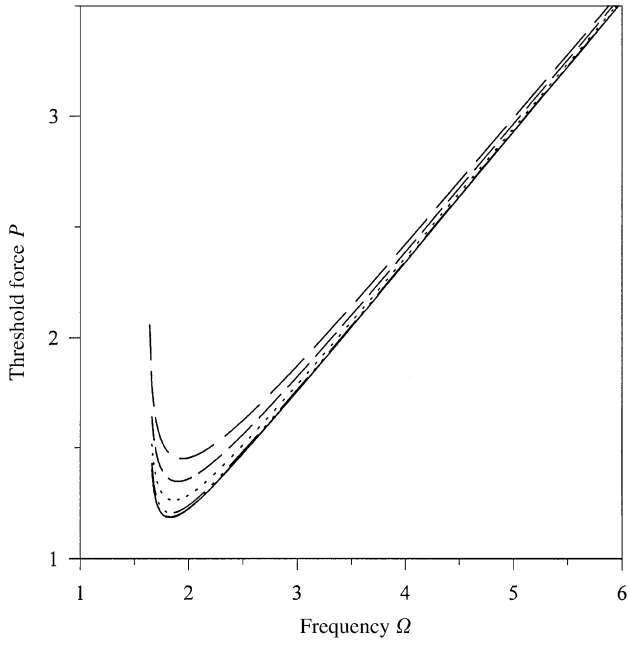

Figure 6. Effect of damping δ on the analytical PDB criterion of the second mode: ———, $\delta = 0{\cdot}02$; —·-, $\delta = 0{\cdot}1$; —··-, $\delta = 0{\cdot}5$; ·····, $\delta = 0{\cdot}75$; – – –, $\delta = 1$.

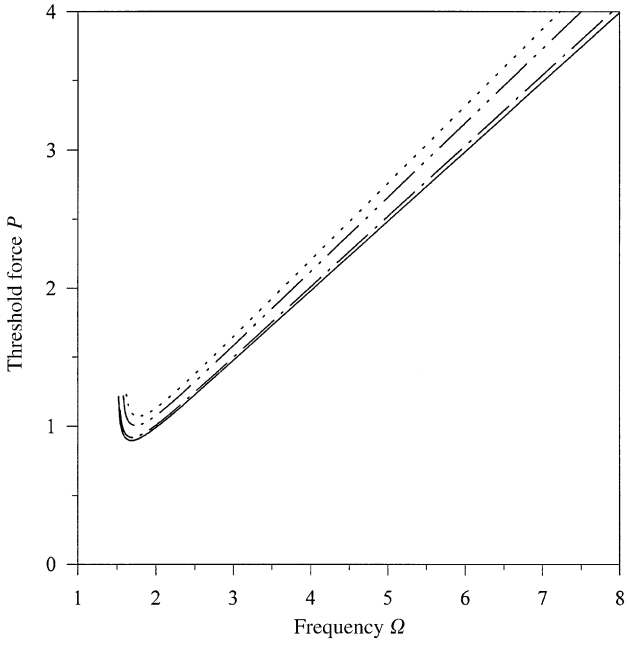

Figure 7. Effect of fluid depth ζ_1 on the analytical PDB criterion of the second mode: ———, $\zeta_1 = 0{\cdot}1$; — ··, $\zeta_1 = 0{\cdot}3$; —··-, $\zeta_1 = 0{\cdot}5$; ·····, $\zeta_1 = 0{\cdot}7$.

On the contrary, in Figures 9 and 10, the threshold force required for PDB decreases as the values of the attached mass magnitude ratio μ and relative position η increase. Results presented in Figure 9 show that increasing the mass ratio μ will decrease the natural

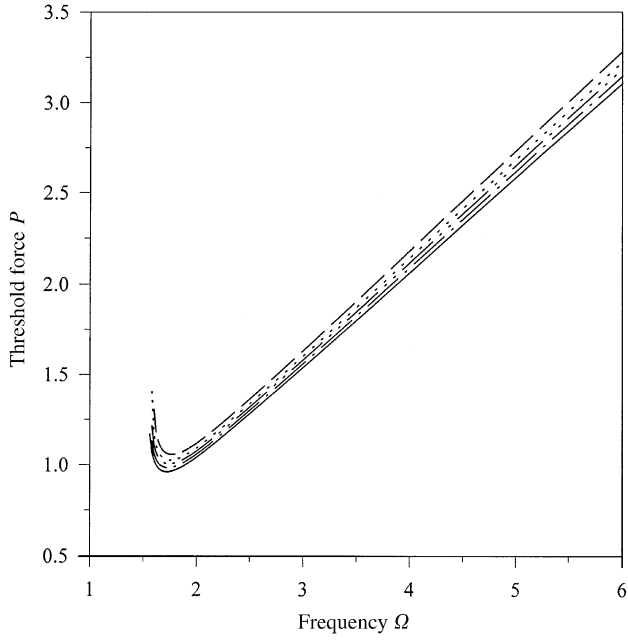

Figure 8. Effect of fluid density ratio K_m on the analytical PDB criterion of the second mode: ——, $K_m = 0{\cdot}6$; —·–, $K_m = 0{\cdot}8$; —··, $K_m = 1{\cdot}0$; ·····, $K_m = 1{\cdot}2$; – – –, $K_m = 1{\cdot}5$.

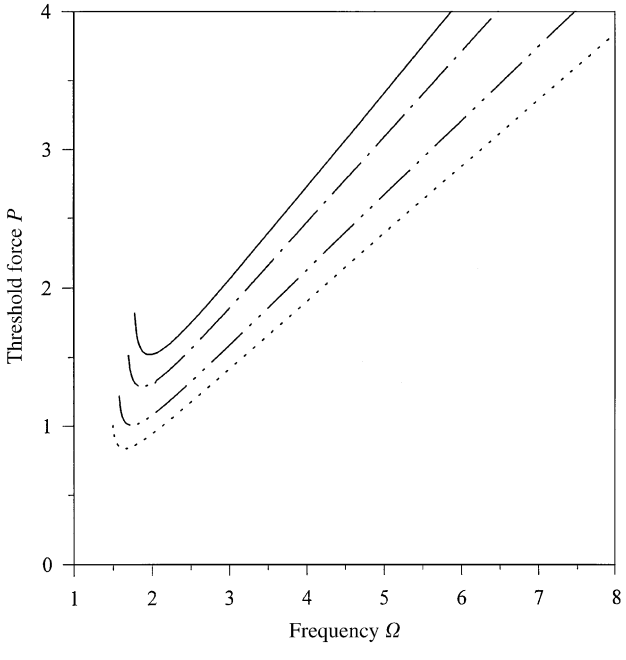

Figure 9. Effect of mass position η on the analytical PDB criterion of the second mode: ———, $\eta = 0{\cdot}55$; —·—, $\eta = 0{\cdot}65$; —··-, $\eta = 0{\cdot}75$; ·····, $\eta = 0{\cdot}85$; – – –, $\eta = 0{\cdot}95$.

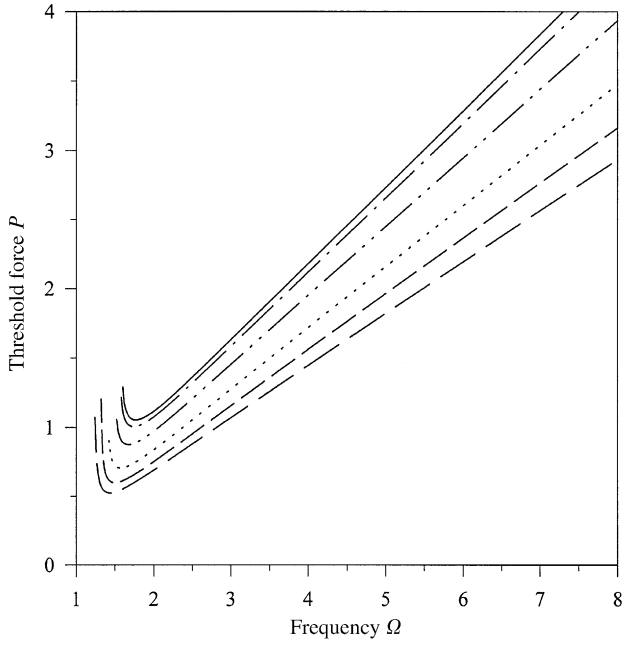

Figure 10. Effect of mass ratio μ on the analytical PDB criterion of the second mode: ———, $\mu = 0{\cdot}10$; —·—, $\mu = 0{\cdot}25$; —··-, $\mu = 0{\cdot}5$; ·····, $\mu = 1{\cdot}0$; – – –, $\mu = 1{\cdot}5$; —–, $\mu = 2{\cdot}0$.

frequencies of the system and decrease the critical bifurcation value of the amplitude, and as a result the critical force required for PDB will decrease. Results presented in Figure 10 show that moving the attached mass towards the free end of the immersed beam makes the beam unstable and consequently the critical force required for PDB decreases.

7. COMPUTER SIMULATION, RESULTS AND DISCUSSION

To verify the results of the approximate theory for the stability analysis and the criterion of PDB, equation (1) was simulated, i.e., integrated by using the Runge–Kutta method, and the results presented in the previous section were verified with the aid of time histories, phase planes, Poincaré maps and Lyapunov fractal dimension.

It was found from computer simulation results for the first mode that by increasing the frequency, the PDB is first observed in the range $0{\cdot}705 < \Omega < 0{\cdot}708$ followed by a $3T$ attractor at $\Omega = 0{\cdot}71$ and chaotic behavior is first observed in the range $0{\cdot}715 < \Omega < 0{\cdot}73$. These frequency bands are in good agreement with the predicted unstable regions of the steady state response curves obtained by using two terms for the second unstable region, Figure 3, at which the PDB and chaos may occur. Results are presented in Figure 11, i.e., the time histories, phase planes and Poincaré maps for some selected values of Ω for the first mode ($P = 10$, $\varepsilon_1 = 1{\cdot}0449$, $\varepsilon_2 = 0{\cdot}9329$, $\delta = 0{\cdot}02$), namely $\Omega = 0{\cdot}707$ and $\Omega = 0{\cdot}72$ at which PDB and chaos occur respectively.

Simulation results for the second mode have shown that, i.e., by increasing the frequency, a higher period doubling $4T$ at $\Omega = 0{\cdot}39$ and a chaotic behavior is observed at $\Omega = 0{\cdot}43$; these results confirm the prediction of the unstable portions of the response curve at which the PDB and chaos can occur. In addition, the PDB is observed in the ranges

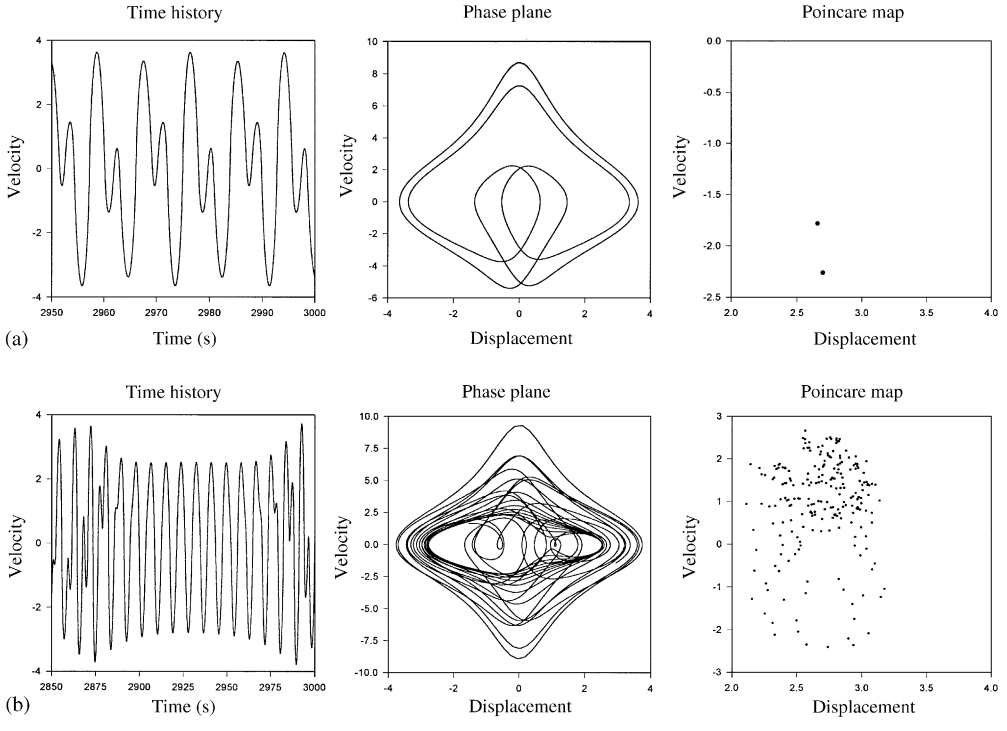

Figure 11. Time history, phase plane and Poincaré map for the first mode. $P = 10, \varepsilon_1 = 1{\cdot}0449, \varepsilon_2 = 0{\cdot}9329$ and $\delta = 0{\cdot}02$, (a) $\Omega = 0{\cdot}707$; (b) $\Omega = 0{\cdot}72$. $\lambda_1 = 0{\cdot}0775, \lambda_2 = 0{\cdot}0, \lambda_3 = -0{\cdot}0839$ and $d_f = 2{\cdot}923$.

$0{\cdot}99 < \Omega < 1{\cdot}1$ and $1{\cdot}9 < \Omega < 2{\cdot}1$, i.e., before entering the second unstable region and inside the second unstable region. In Figure 12, the time histories, phase planes and Poincaré maps are shown for two values of Ω selected from the predicted frequency bands of the second mode and for the parameters $P = 2{\cdot}5$, $\varepsilon_1 = 5.7882$, $\varepsilon_2 = 1{\cdot}2546$, $\delta = 0{\cdot}02$.

As for the third mode, computer simulation results have shown also that the PDB is first observed at $\Omega = 0{\cdot}2$ followed by a attractor $3T$ at $\Omega = 0{\cdot}21$ and a chaotic behavior is observed at $\Omega = 0{\cdot}29$. The second PDB is observed in the range $0{\cdot}69 < \Omega < 0{\cdot}76$, followed by a $3T$ attractor and ends with higher period doublings $4T$ at $\Omega = 0{\cdot}89$. The first chaotic zone observed is in the range $1.15 < \Omega < 1{\cdot}3$ and then ends with a $9T$ attractor at $\Omega = 1{\cdot}35$, followed by a $3T$ attractor at $\Omega = 1{\cdot}40$. The $3T$ attractor disappears and the chaos returns in the ranges $1{\cdot}80 < \Omega < 2{\cdot}0$ and $2{\cdot}15 < \Omega < 2{\cdot}3$. Further investigations showed that the third PDB zone is in the range $2{\cdot}6 < \Omega < 3{\cdot}0$ and at $\Omega > 3{\cdot}0$ periodicity returns to the system.

In Figure 13, the time histories, phase planes and Poincaré maps are shown for different values of Ω, for the third mode, i.e., $P = 3{\cdot}5$, $\varepsilon_1 = 10{\cdot}9587$, $\varepsilon_2 = 1{\cdot}1258$, $\delta = 0{\cdot}1$. Results presented in Figure 5 and with the aid of computer simulations in Figure 13 show that, as one may expect, the resonance curves of the asymmetric solution intersect those of the symmetric solution near the region of chaotic motion, which lies in the zone where the resonance curves of the symmetric solution may enter the second unstable region [20].

Chaotic behavior of the non-linear temporal unimodal equation of motion is verified also by another diagnostic tool which is used in dynamical systems, the calculation of Lyapunov exponents. In the present work the Lyapunov exponents are calculated, by using the algorithm presented by Wolf *et al.* [28], from the generated time histories, i.e., by integrating

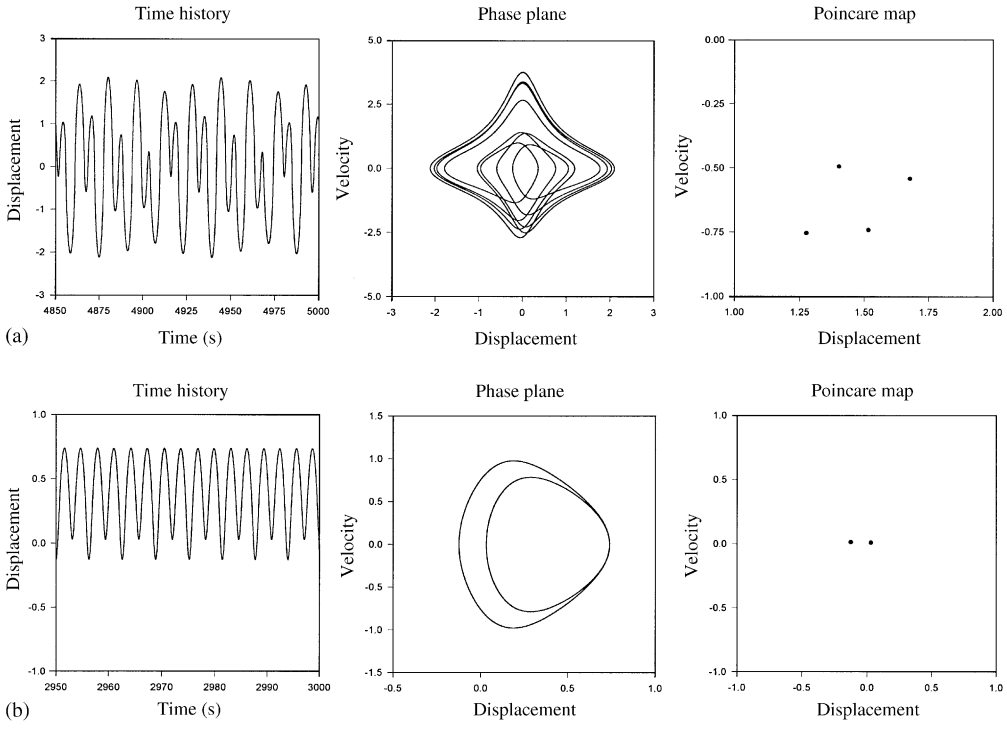

Figure 12. Time history, phase plane and Poincaré map for the second mode. $P = 2{\cdot}5$, $\varepsilon_1 = 5{\cdot}7882$, $\varepsilon_2 = 1{\cdot}2546$ and $\delta = 0{\cdot}02$. (a) $\Omega = 0{\cdot}39$; (b) $\Omega = 2{\cdot}0$.

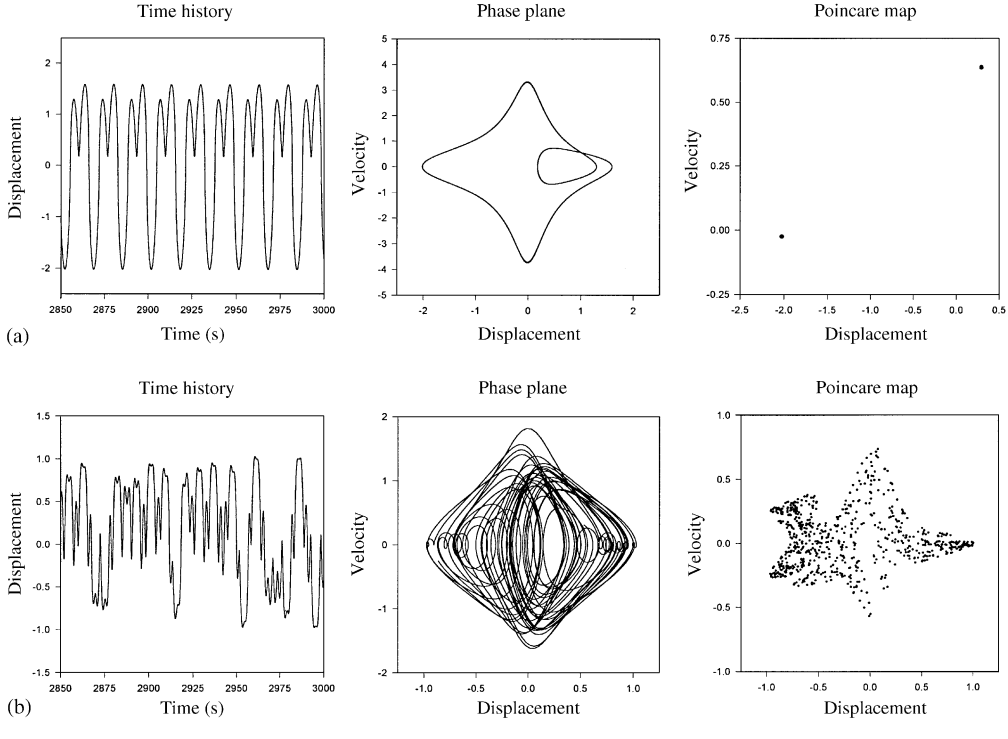

Figure 13. Time history, phase plane and Poincaré map for the third mode. $P = 3{\cdot}5$, $\varepsilon_1 = 10{\cdot}9587$, $\varepsilon_2 = 1{\cdot}1258$ and $\delta = 0{\cdot}1$. (a) $\Omega = 0{\cdot}76$; (b) $\Omega = 2{\cdot}3$, $\lambda_1 = 0{\cdot}3497$, $\lambda_2 = 0{\cdot}0$, $\lambda_3 = -0{\cdot}3783$ and $d_f = 2{\cdot}924$.

equation (1) using the Runge–Kutta method. The signs of the Lyapunov exponents provide a qualitative picture of a system's dynamics. In a three-dimensional continuous dissipative dynamical system the only possible values of the Lyapunov exponents for chaos are to be positive, zero and negative [28]. To summarize, any chaotic attractor defined in a 3-D phase space will have $\lambda_1 > 0$, $\lambda_2 = 0$ and $\lambda_3 < 0$ with $\sum \lambda_i < 0$ where λ_1, λ_2 and λ_3 are the Lyapunov exponents [28–30].

The connection between the fractal dimension of a chaotic attractor and the Lyapunov exponents that characterize the attractor is given by the relation [28–30]

$$d_f = n + \frac{\sum_{i=1}^{n} \lambda_i}{|\lambda_{n+1}|}, \tag{22}$$

where the Lyapunov exponents are ordered from largest to smallest ($\lambda_1 > \lambda_2 > \cdots > \lambda_n$) and n is the largest integer having the property that $\lambda_1 + \lambda_2 + \cdots + \lambda_n > 0$, i.e., $\sum_{i=1}^{n} \lambda_i > 0$ or $\sum_{i=1}^{n+1} \lambda_i < 0$. In the case of a chaotic behavior in a 3-D phase space, which is the case for the present work, equation (21) reduces to

$$d_f = 2 + \frac{\lambda_1}{|\lambda_3|}, \tag{23}$$

upon noting that $\lambda_1 > 0$, $\lambda_2 = 0$ and $\lambda_3 < 0$, so that $d_f > 2$.

On the presented Poincaré maps in Figures 11–13 that have chaotic behavior, the calculated Lyapunov exponents and the fractal dimensions are shown to be used as a diagnostic tool for chaos.

To compare the results obtained for the criterion of PDB, in Figures 14 and 15, the proposed criterion is shown with the true boundaries of PDB and chaos for the second and

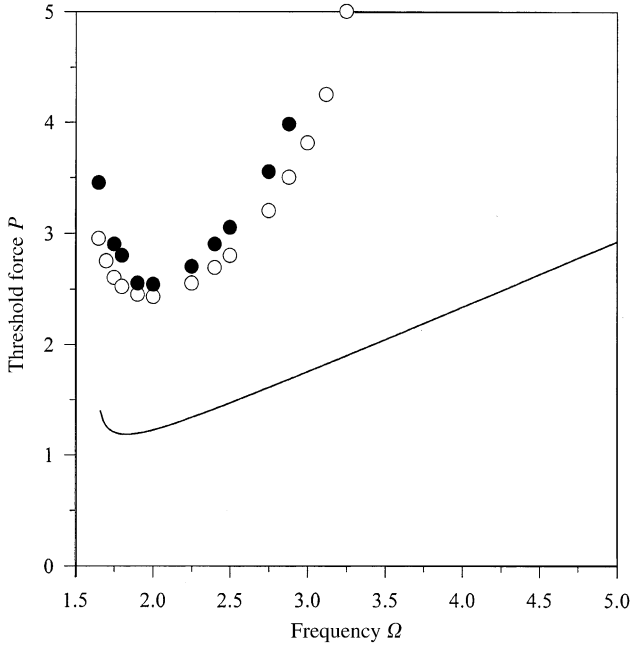

Figure 14. Analytical PDB criterion obtained by using equation (34) for the second mode, true PDB and true chaotic boundaries. $P = 2{\cdot}5$, $\varepsilon_1 = 5{\cdot}7882$, $\varepsilon_2 = 1{\cdot}2546$ and $\delta = 0{\cdot}02$: ————, analytical PDB; ○, true PDB; ●, true chaos.

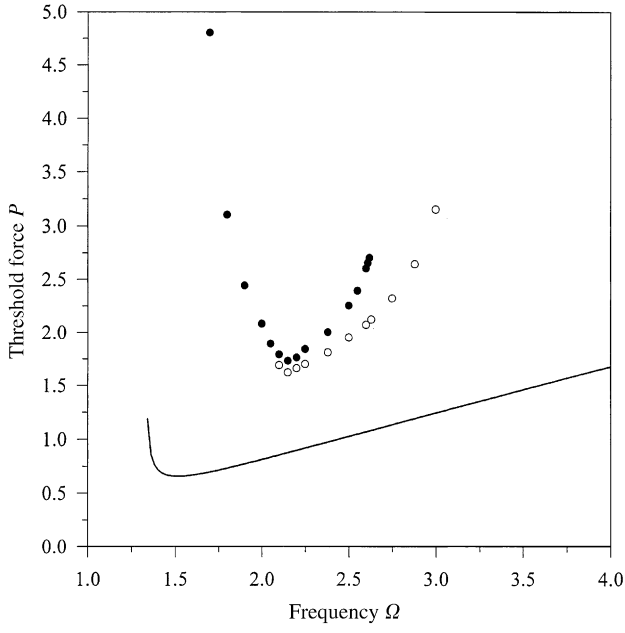

Figure 15. Same as in Figure 14 but for the third mode.

third modes respectively. The difference between the proposed criterion and the true boundary of PDB is due to the fact that it is calculated by using a single term only in the assumed solution. On the other hand, the boundaries of the true PDB and chaos have the same qualitative characteristics and they give the minimum threshold values for both PDB and chaos.

To verify the results presented in Figure 15 for the third mode, i.e., $\varepsilon_1 = 10{\cdot}9587$, $\varepsilon_2 = 1{\cdot}1258$, $\delta = 0{\cdot}1$, for the true boundaries of PDB and chaos time histories, phase planes and Poincaré maps are shown in Figure 16, for $\Omega = 2{\cdot}25$ and for different values of P. These results show that the behavior is periodic at $P = 1{\cdot}69$, PDB at $P = 1{\cdot}70$, higher period doublings ($4T$) at $P = 1{\cdot}85$ and chaos appears at $P = 1{\cdot}86$. This confirms that the PDB may be considered to be the lower threshold of chaos in some dynamical systems [20].

8. CONCLUSIONS

The present work studied the resonance response curves, second order stability analysis, asymmetric solutions and their stabilities for an extensible immersed cantilever beam system as shown in Figure 1, for the first three modes of vibration. The results presented indicate that for the type of non-linear oscillators governed by equation (1), which belongs to the general class of non-linear oscillators studied in reference [20], the two-term harmonic solutions of the resonance response and second order stability analysis of the associated linearized variational Hill-type equation may predict with good accuracy the portions on the resonance response curves at which the period-doubling bifurcation (PDB) may arise, for different physical system parameters corresponding to the first three modes.

Also shown has been the effect of the physical parameters of the system, i.e., the attached mass magnitude ratio μ, relative position η, relative depth ζ_1 of the immersed part, fluid density parameter K_m and the damping δ, on the bifurcation diagram of the beam–mass

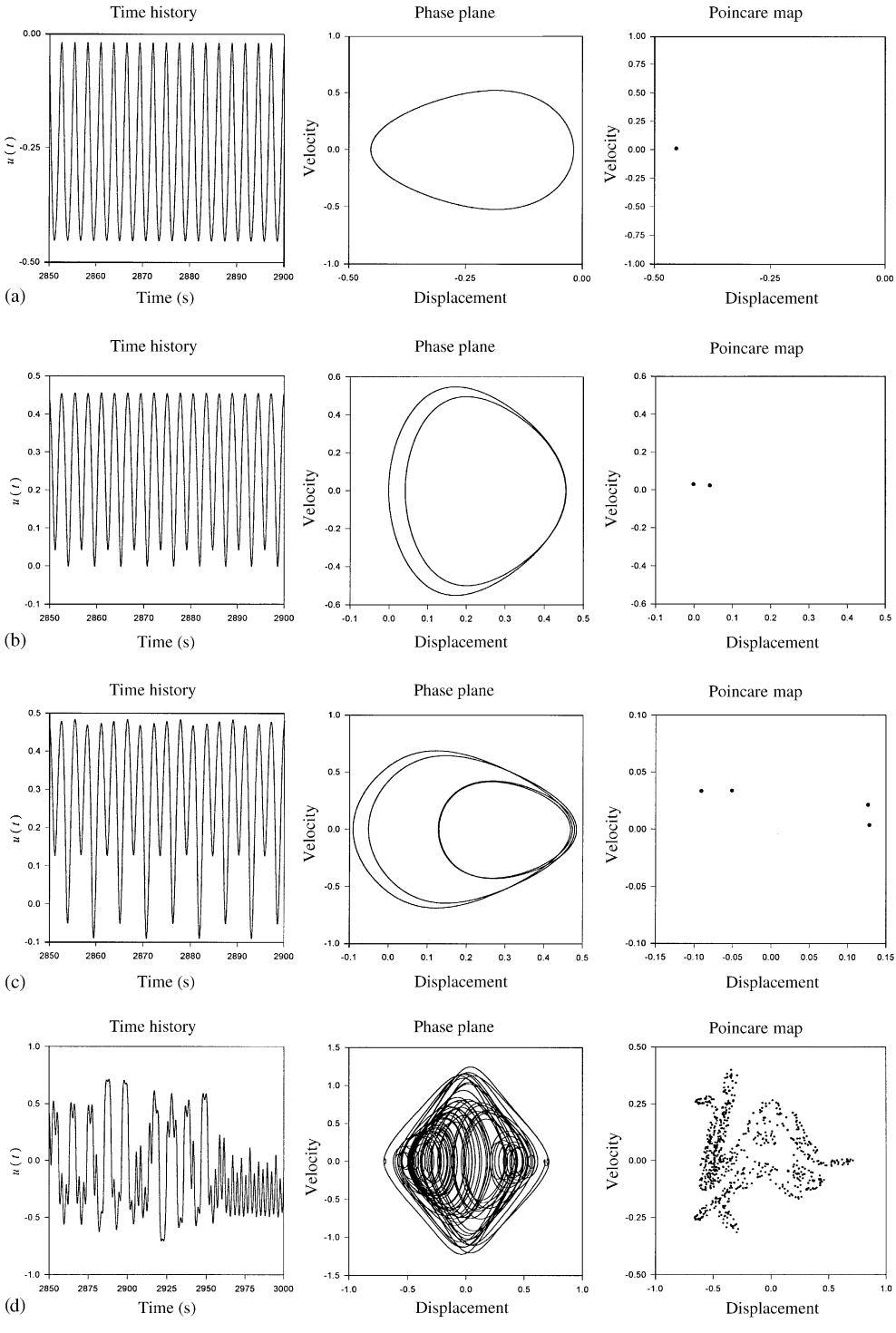

Figure 16. Time history, phase plane and Poincaré map for the third mode, $\varepsilon_1 = 10{\cdot}9587$, $\varepsilon_2 = 1{\cdot}1258$, $\delta = 0{\cdot}1$ and $\Omega = 2{\cdot}25$ but for different values of the excitation amplitude P. (a) $P = 1{\cdot}69$; (c) $P = 1{\cdot}70$; (d) $P = 1{\cdot}85$; (e) $P = 1{\cdot}86$, $\lambda_1 = 0{\cdot}2733$, $\lambda_2 = 0{\cdot}0$, $\lambda_3 = -0{\cdot}3156$ and $d_f = 2{\cdot}866$.

system and on the critical excitation amplitude P_{cr}: i.e., P_{cr} increases by increasing δ, ζ_1 and K_m and P_{cr} decreases by increasing μ and η.

ACKNOWLEDGMENTS

The authors would like to acknowledge the support of both the Deanship of Scientific Research, University of Jordan, Amman, Jordan and King Fahd University of Petroleum and Mineral, Dhaharan, Saudi Arabia.

REFERENCES

1. A. NAYFEH 2000 *Nonlinear Interaction*: *Analytical, Computational and Experimental Methods*. New York: John Wiley & Sons.
2. W. SZEMPLINSKA-STUPNICKA 1986 *International Journal of Nonlinear Mechanics* **23**, 257–277. Bifurcations of harmonic solution leading to chaotic motion in the softening type Duffing's oscillator.
3. W. SZEMPLINSKA-STUPNICKA 1987 *Journal of Sound and Vibration* **113**, 155–172. Secondary resonance and approximate models of rout to chaotic motion in non-linear oscillators.
4. W. SZEMPLINSKA-STUPNICKA and J. BAJKOWSKI 1986 *International Journal of Non-Linear Mechanics* **21,** 401–419. The 1/2 subharmonic resonance and its transition to chaotic motion in a non-linear oscillator.
5. J. C. HUANC, Y. H. KAO, C. S. WANG and Y. GOU 1989 *Physics Letters A* **136**, 131–138. Bifurcation structure of the Duffing oscillator with asymmetric potential well.
6. K. L. LIU and K. YOUNG 1986 *Journal of Mathematics and Physics* **27**, 502–506. Stability of forced nonlinear oscillators via Poincaré map.
7. JHERATH and K. FESSER 1987 *Physical Letters A* **120**, 265–268. Mode expansions and bifurcations in nonlinear single-well oscillators.
8. A. H. NAYFEH and N. E. SANCHEZ 1989 *International Journal of Non-linear Mechanics* **24**, 483–497. Bifurcations in a forced softening Duffing oscillator.
9. Z. RAHMAN and T. D. BURTON 1986 *Journal of Sound and Vibration* **110**, 363–380. Large amplitude primary superharmonic resonances in the Duffing oscillator.
10. W. SZEMPLINSKA-STUPNIKA 1994 *Journal of Sound and Vibration* **178**, 276–284. A discussion of an analytical method of controlling chaos in Duffing oscillator.
11. A. HASSAN 1994 *Journal of Sound and Vibration* **172**, 513–526. On the third superharmonic resonance in the Duffing oscillator.
12. B. A. HUBERMAN and J. P. CRUTCHFIELD 1979 *Physica Review Letters* **43**, 1743–1747. Chaotic states of anharmonic systems in periodic fields.
13. R. RATY, J. VON BOEHM and H. M. ISOMAKI 1984 *Physical Letters A* **103**, 289–292. Absence of inversion-symmetric limit cycles of even periods and chaotic motion of Duffing oscillator.
14. R. VAN DOOREN 1988 *Journal of Sound and Vibration* **23**, 327–339. On the transition from regular to chaotic behavior in the Duffing oscillator.
15. M. N. HAMDAN and T. D. BURTON 1993 *Journal of Sound and Vibration* **166**, 255–266. On the steady state response and stability of non-linear oscillators using harmonic balance.
16. K. R. ASFAR and K. K. MASOUD 1992 *Journal of Vibration and Acoustics* **144**, 489–494. On the period-doubling bifurcations in the Duffing's oscillator with negative linear stiffness.
17. J. AWREJCEWICZ and J. MROZOWSKI 1989 *Journal of Sound and Vibration* **89**, 89–100. Bifurcation and chaos of a particular Van Der Pol–Duffing oscillator.
18. L. D. ZAVODNEY, A. H. NAYFEH and N. E. SANCHEZ 1989 *Journal of Sound and Vibration* **129**, 417–442. The response of a single-degree-of-freedom system with quadratic and cubic non-linearities to a principal parametric resonance.
19. A. HASSAN 1996 *Nonlinear Dynamics* **10**, 105–133. On the local stability analysis of the approximate harmonic balance solutions.
20. A. A. AL-QAISIA and M. N. HAMDAN 2001 *Journal of Sound and Vibration* **244**, 453–479. Bifurcation of approximate harmonic balance solution and transition to chaos in an oscillator with inertial and elastic symmetric nonlinearities.
21. A. A. AL-QAISIA, B. O. AL-BEDOOR and M. N. HAMDAN 2000 *Shock and Vibration* **7**, 179–194. On the steady state response of a cantilever beam partially immersed in a fluid and carrying an intermediate mass.

22. L. D. ZAVODNEY and A. H. NAYFEH 1989 *International Journal of Nonlinear Mechanics* **24**, 105–125. The nonlinear response of a slender beam carrying a lumped mass to a principal parametric excitation: theory and experiment.
23. M. R. M. CRESPO DA SILVA and C. C. GLYNN 1978 *Journal of Structural Mechanics* **6,** 437–448. Nonlinear flexural–flexural–torsional dynamics of inextensible beams, I: equations of motion.
24. M. N. HAMDAN and N. H. SHABANEH 1997 *Journal of Sound and Vibration* **199**, 737–750. On the period of large amplitude free vibrations of conservative autonomous oscillators with static and inertia nonlinearities.
25. H. N. ARAFAT, A. H. NAYFEH and C. CHIN 1998 *Nonlinear Dynamics* **15**, 31–61. Nonlinear nonplanar dynamics of parametrically excited cantilever beams.
26. J. Y. CHANG and W. H. LIU 1989 *Journal of Sound and Vibration* **130**, 516–524. Some studies on the natural frequencies of immersed restrained column.
27. A. A. AL-QAISIA and M. N. HAMDAN 1999 *Journal of Sound and Vibration* **223**, 49–71. On the steady state response of oscillators with static and inertia non-linearities.
28. A. WOLF, J. B. SWIFT, H. L. SWINNEY and J. A. VASTANO 1985 *Physica D* **16**, 285–317. Determining Lyapunov exponent from a time series.
29. F. C. MOON 1987 *Chaotic Vibrations*. New York: John Wiley & Sons.
30. T. D. BURTON 1994 *Introduction to Dynamic Systems Analysis*. New York: McGraw-Hill.
31. B. O. AL-BEDOOR and Y. KHULIEF 1997 *Journal of Sound and Vibration* **206**, 641–661. General planar dynamics of a sliding flexible link.
32. S. W. SHAW 1988 *Journal of Sound and Vibration* **124**, 329–343. Chaotic dynamics of a slender beam rotating about its longitudinal axis.

APPENDIX A: DERIVATION OF EQUATION OF MOTION

A.1. SYSTEM DESCRIPTION AND ASSUMPTIONS

A schematic of the beam under study is shown in Figure 1. The beam is considered to be uniform of constant length l, cross-sectional area A, flexural rigidity EI and density ρ. The beam is vertically mounted, clamped at the base and partially immersed in a fluid up to depth l_1 and carries a lumped mass M at an arbitrary intermediate position d along the beam span. The fluid is assumed to be non-viscous, incompressible with a constant density ρ'. The thickness of the beam is assumed to be small compared to the length of the beam, so the effect of rotary inertia and shear deformation can be ignored.

The beam considered is assumed to be slender. Such slender beam systems may undergo large bending motion without a significant axial deformation and therefore are assumed to be inextensible and the natural frequencies of the axial motion are much higher than those of the bending motion. An obvious exception of the inextensibility condition is the large-amplitude vibrations of beams mounted between two fixed points, since in such a case the inextensibility condition is violated. This modelling approach is similar to that considered by Zavodney and Nayfeh [22], Crespo da Silva and Glynn [23], Hamdan and Shabaneh [24], Al-Qaisia *et al.* [21] and Arafat *et al.* [25].

Also, the beam is subjected to a concentrated transverse harmonic load at an arbitrary point along its span. In addition, the effect of axial inertia and non-linear curvature were taken into consideration and the fluid–structure interaction can be taken as an added inertia to the structure [26].

A.2. EQUATION OF MOTION

Upon using the co-ordinate system shown in Figure 1 for the immersed beam, the elastic potential energy V_e of the beam due to bending is given by

$$V_e = \frac{EIl}{2} \int_0^1 R^2\,(\zeta)\,\mathrm{d}\zeta, \tag{A1}$$

where $\zeta = s/l$ is the dimensionless arc length and $R(\zeta)$ is the curvature of the beam neutral axis. The exact curvature $R(\zeta)$ takes the form [22]

$$R = \lambda\phi', \tag{A2}$$

where $\sin\phi = \lambda y'$. Differentiating equation (A2) and noting that $\cos\phi = \sqrt{1 - \sin^2\phi}$ and substituting into equation (A2), one obtains the following expression for the curvature of the beam [22]:

$$R = \lambda^2 y''/\sqrt{1 - (\lambda y')^2}, \tag{A3}$$

where $\lambda = 1/l$ and the prime denotes differentiation with respect to the non-dimensional arc length ζ. The system potential energy must contain the gravitational potential energy developed as a result of axial shortening due to transverse deformations. An expression for the axial shortening based on the assumption of no axial deflection [31] is

$$\mathrm{d}\delta \cong -\frac{1}{2}\left(\frac{\partial y}{\partial s}\right)^2. \tag{A4}$$

The gravitational potential energy of the system, upon using equation (A4), can be written as

$$V_g = -\rho A l g \int_0^1 \left(\int_0^\zeta \lambda^2 \frac{y'^2}{2}\,\mathrm{d}\chi\right)\mathrm{d}\zeta - Mg\int_0^\eta \frac{\lambda^2}{2}\,y'^2\,\mathrm{d}\zeta, \tag{A5}$$

where M is the lumped mass located at the position $\eta = \mathrm{d}/l$. The resulting potential energy of the system can be obtained by adding equation (A5) to (A1): i.e.

$$V = \frac{EI\lambda^3}{2}\int_0^1 (y''(1 - (\lambda y')^2)^{-1/2})^2\,\mathrm{d}\zeta - \rho A l g\int_0^1 \left(\int_0^\zeta \lambda^2\frac{y'^2}{2}\,\mathrm{d}\chi\right)\mathrm{d}\zeta - Mg\int_0^\eta \frac{\lambda^2}{2}\,y'^2\,\mathrm{d}\zeta. \tag{A6}$$

Upon expanding the term $(1 - \lambda^2\gamma'^2)^{-1}$ into a power series and noting that $(\lambda^2 y'^2) < 1$, equation (A6) becomes when the non-linear terms are retained up to fourth order

$$V = \frac{EI\lambda^3}{2}\int_0^1 [y''^2 + (\lambda y' y'')^2]\,\mathrm{d}\zeta - \frac{\rho A l g}{2}\left\{\int_0^1\int_0^\zeta (\lambda y'^2)\,\mathrm{d}\chi\,\mathrm{d}\zeta - \mu\int_0^1 (\lambda y'^2)\,\mathrm{d}\zeta\right\}, \tag{A7}$$

where $\mu = M/\rho A l$.

Next, the kinetic energy T of the system is given by

$$T = \frac{\rho A}{2}(1 + C_m K_m)\int_0^{l_4} (\dot{x}^2 + \dot{y}^2)\,\mathrm{d}s + \frac{\rho A}{2}\int_{l_1}^1 (\dot{x}^2 + \dot{y}^2)\,\mathrm{d}s + \tfrac{1}{2}M(\dot{x}^2 + \dot{y}^2)_{s=d}, \tag{A8}$$

where C_m is the inertia coefficient of the additional mass of the fluid and $K_m = \rho'/\rho$ as imposed by Chang and Liu [26]. Note that the system kinetic energy in equation (A8) is a function of the velocity variables $\dot{x}$ and $\dot{y}$. The axial velocity $\dot{x}$ can be eliminated from this equation by noting that for the present inextensible planar beam motion, i.e., no extension of the beam's neutral axis, the inextensibility condition can be derived as follows [25].

Before deformation the position of a point on the elastic axis is given by $\mathbf{r}_0 = s\mathbf{e}_x$. After deformation, its position is given by $\mathbf{r} = (s + x)\mathbf{e}_{x'} + y\mathbf{e}_{y'}$, where $\mathbf{e}_x$, $\mathbf{e}_{x'}$ and $\mathbf{e}_{y'}$ are the unit

vectors before and after deformation. Hence, the strain along the elastic axis of a differential element is defined by

$$e = \left(\frac{\partial \mathbf{r}}{\partial s}\cdot\frac{\partial \mathbf{r}}{\partial s}\right)^{1/2} - \left(\frac{\partial \mathbf{r}_0}{\partial s}\cdot\frac{\partial \mathbf{r}_0}{\partial s}\right)^{1/2} = \sqrt{(1+\lambda x')^2 + (\lambda y')^2} - 1. \tag{A9}$$

For inextensional beams, the elongation e is assumed to be zero, resulting in the condition [22, 23, 25]

$$(1+\lambda x')^2 + (\lambda y')^2 = 1. \tag{A10}$$

The inextensibility condition (A10) allows one to relate, through consistent geometric consideration, the axial and the lateral displacement and thus remove the axial motion from the system kinetic energy (A8).

Equation (A10) may be written as $1 + \lambda x' = [1 - (\lambda y')^2]^{1/2}$, where a prime denotes a derivative with respect to the dimensionless arc length ζ. Then, noting that $(\lambda^2 y'^2) < 1$, expanding the right-hand side into a power series, retaining non-linear terms up to the desired (i.e., fourth) order, and integrating the result from 0 to an arbitrary value of ζ leads to the following expression for the axial displacement (shortening) x due to the flexural bending y:

$$x = -\frac{1}{2}\int_0^{\zeta} (\lambda y'^2 + \tfrac{1}{4}\lambda^3 y'^4)\,\mathrm{d}\chi. \tag{A11}$$

Differentiating with respect to time t, squaring and retaining the non-linear terms up to fourth order leads to

$$\dot{x}^2 = \frac{1}{4}\left[\left(\int_0^{\zeta} (\lambda y'^2 + \tfrac{1}{4}\lambda^3 y'^4)\,\mathrm{d}\chi\right)^{\cdot}\right]^2. \tag{A12}$$

Upon substituting equation (A11) into equation (A8), the system kinetic energy T of the beam system considered becomes

$$T = \frac{\rho A l}{2}\left\{\left(\int_0^1 \left(\dot{y}^2 + \tfrac{1}{4}\left(\left[\left(\int_0^{\zeta} \lambda y'^2\,\mathrm{d}\chi\right)^{\cdot}\right]^2\right)\right)\mathrm{d}\zeta\right)\right\} + \frac{\rho A l}{2} C_m K_m \int_0^{\zeta_1}\left(\dot{y}^2 + \tfrac{1}{4}\left[\left(\int_0^{\zeta} \lambda y'^2\,\mathrm{d}\chi\right)^{\cdot}\right]^2\right)\mathrm{d}\zeta$$
$$+ \frac{\rho A l}{2}\mu\left[\dot{y}^2 + \tfrac{1}{4}\left[\left(\int_0^{\zeta} \lambda y'^2\,\mathrm{d}\chi\right)^{\cdot}\right]^2\right]\Bigg|_{\zeta=\eta}, \tag{A13}$$

where $\zeta_1 = l_1/l$. Using equations (A7) and (A12) one obtains, after factoring out $\rho A l/2$, the system Lagrangian $L = T - V$, as

$$L = \frac{\rho A l}{2}\left\{\int_0^1 \left(\dot{y}^2 + \tfrac{1}{4}\left(\left[\left(\int_0^{\zeta} \lambda y'^2\,\mathrm{d}\chi\right)^{\cdot}\right]^2\right)\right)\mathrm{d}\zeta + C_m K_m \int_0^{\zeta_1}\left(\dot{y}^2 + \tfrac{1}{4}\left[\left(\int_0^{\zeta} \lambda y'^2\,\mathrm{d}\chi\right)^{\cdot}\right]^2\right)\mathrm{d}\zeta\right.$$
$$\left. + \mu\left[\dot{y}^2 + \tfrac{1}{4}\left[\left(\int_0^{\zeta} \lambda y'^2\,\mathrm{d}\chi\right)^{\cdot}\right]^2\right]\Bigg|_{\zeta=\eta}\right\} - \beta^2\int_0^1 (y''^2 + (\lambda y' y'')^2)\,\mathrm{d}\zeta$$
$$+ g_0\left[\int_0^1\int_0^{\zeta} (\lambda y'^2)\,\mathrm{d}\chi\,\mathrm{d}\zeta + \mu\int_0^1 (\lambda y')\,\mathrm{d}\zeta\right], \tag{A14}$$

where $\beta^2 = EI\lambda^3/\rho Al$ is the linear frequency parameter and $g_0 = \rho Al^3 g/EI$ is the dimensionless gravity parameter.

The continuous system in equation (A14) does not admit a closed-form solution. However, the interest here is in the case where the immersed beam motion is dominated by a single active mode and it is assumed that the modal subspaces are invariant and individually active [32]. Therefore, an approximate solution will be sought that satisfies both the equation and the boundary conditions. Since the boundary conditions are spatial and independent of time, an assumed single-mode approach may be used to discretize the continuous Lagrangian, by any of the variational methods such as Rayleigh–Ritz. When the assumed function is the eigenfunction in particular, the procedure is known as Galerkin's method [22]. Accordingly, one assumes

$$y(\zeta, \tau) = \phi(\zeta) q(\tau), \tag{A15}$$

where $q(\tau)$ is an unknown time modulation of the assumed mode shape and $\phi(\zeta)$ is the normalized mode shape function of the linear cantilever beam, i.e., $\int_0^1 \phi^2(\zeta)\,\mathrm{d}\zeta = 1$, which is assumed to remain self-similar (i.e., independent of motion amplitude) during the motion. In this work Galerkin's method is used, whereby $\phi(\zeta)$ is the eigenfunction of the nth mode of the cantilever beam, given in many vibration text books as

$$\phi(\zeta) = (\cosh p\zeta - \cos p\zeta) + \frac{\cos p + \cosh p}{\sin p + \sinh p}(\sin p\zeta - \sinh p\zeta), \tag{A16}$$

where p is the nth root of the frequency equation $1 + \cos p \cosh p = 0$. The first four roots of this equation are 1·875104, 4·694091, 7·854757 and 10·99554.

Substituting equation (A15) into equation (A14), one obtains the discrete beam Lagrangian, which can be expressed as

$$L = \frac{\rho Al}{2}[\alpha_1 \dot{q}^2 - \alpha_2 \beta^2 q^2 + \alpha_3 \lambda^2 \dot{q}^2 q^2 - \alpha_4 \beta^2 \lambda^2 q^4], \tag{A17}$$

where

$$\alpha_1 = \int_0^1 \phi^2 \mathrm{d}\zeta + C_m k_m \int_0^{\zeta_1} \phi^2 \,\mathrm{d}\zeta + \mu\phi^2, \tag{A18}$$

$$\alpha_2 = \int_0^1 \phi''^2 \mathrm{d}\zeta - g_0 \int_0^1 \left(\int_0^\zeta \phi'^2 \,\mathrm{d}\chi\right)\mathrm{d}\zeta - g_0 \mu \int_0^\eta \phi'^2 \,\mathrm{d}\zeta, \tag{A19}$$

$$\alpha_3 = \int_0^1 \left(\int_0^\zeta \phi'^2 \mathrm{d}\chi\right)^2 \mathrm{d}\zeta + C_m k_m \int_0^{\zeta_1} \left(\int_0^\zeta \phi'^2 \,\mathrm{d}\chi\right)^2 \mathrm{d}\zeta + \mu\left[\int_0^\zeta \phi'^2 \,\mathrm{d}\chi\right]_{\zeta=\eta}, \tag{A20}$$

$$\alpha_4 = \int_0^1 \phi'^2 \phi''^2 \,\mathrm{d}\zeta. \tag{A21}$$

To study the forced planar response of the beam system a concentrated load $F_0 \cos(\bar{\Omega}\tau)$ acting at an arbitrary ζ_c along the span of the beam is assumed to act only in the y direction: i.e., the beam transverse direction. Upon the application of the Euler–Lagrange equation

$$Q = \frac{\partial}{\partial t}\left(\frac{\partial L}{\partial \dot{q}}\right) - \frac{\partial L}{\partial q}, \tag{A22}$$

where Q is the generalized force, which can be determined from the principle of virtual work method, $\delta W = Q\delta y$, one obtains the discrete beam non-linear equation as

$$\alpha_1\ddot{q} + \beta^2\alpha_2 q + \alpha_3\lambda^2 q^2\ddot{q} + \alpha_3\lambda^2 q\dot{q}^2 + 2\beta^2\lambda^2\alpha_4 q^3 = \alpha_5\frac{F_0}{\rho A l}\cos(\bar{\Omega}\tau), \tag{A23}$$

where $\alpha_5 = \phi(\zeta_c)$. It is to be noted that some of the coefficients α_i in equations (A18–A21) increase sharply and attain relatively large values at the higher modes of the beam. Therefore, for convenience, equation (A22) is scaled and converted to the dimensionless form

$$\ddot{u} + u + \varepsilon_1 u^2\ddot{u} + \varepsilon_1 u\dot{u}^2 + \varepsilon_2 u^3 = \varepsilon_3\bar{F}\cos(\Omega t), \tag{A24}$$

where

$$\varepsilon_1 = \alpha_3/p^2\alpha_1,\ \varepsilon_2 = 2\alpha_4/p^2\alpha_2,\ \varepsilon_3 = p\alpha_5/\alpha_2 \text{ and } \bar{F} = \frac{F_0}{\rho A l^2\beta^2}. \tag{A25}$$

Dots now denote derivatives with respect to the dimensionless time $t = \beta(\alpha_2/\alpha_1)^{1/2}\tau$, $\Omega = \bar{\Omega}/\beta(\alpha_2/\alpha_1)^{1/2}$, $u = pq/l$ is the dimensionless displacement amplitude at the point of maximum deflection, and $p^2 = \omega/\beta$ is the dimensionless frequency, and ω is the frequency of the assumed mode of the associated linear cantilever beam.

For some stability analysis, structure and water effective damping are assumed to be viscous, with damping coefficient δ, which can be added to the equation of motion to take the form

$$\ddot{u} + \delta\dot{u} + u + \varepsilon_1 u^2\ddot{u} + \varepsilon_1 u\dot{u}^2 + \varepsilon_2 u^3 = P\cos(\Omega t), \tag{A26}$$

where $P = \varepsilon_3\bar{F}$. Equation (A26) belongs to the same class of nonlinear oscillators studied recently by Al-Qaisia and Hamdan [20].

APPENDIX B: HARMONIC BALANCE SOLUTION

B.1. SINGLE-TERM HARMONIC SOLUTION (SHB)

According to the HB method, an approximate solution of equation (2) takes the form

$$u(T) = A\cos T, \tag{B1}$$

where A is the steady state response amplitude. Substituting equation (B1) into equation (2), neglecting third harmonics that arise, and equating coefficients of first harmonics, one obtains the following equations:

$$\left(\frac{3}{4}\varepsilon_2 - \frac{\varepsilon_1}{2}\Omega^2\right)A^3 + (1 - \Omega^2)A = P\cos\phi, \tag{B2}$$

$$\Omega\delta A = P\sin\phi. \tag{B3}$$

The steady state frequency response is obtained by squaring and adding equations (B2) and (B3) and solving for Ω^2 as a function of A; this yields the steady state frequency response:

$$\Omega^4(4\varepsilon_1^2A^6 + \varepsilon_1A^4 + A^2) + \Omega^2((\delta^2 - 2)A^2 - (\tfrac{3}{2}\varepsilon_2 + \varepsilon_1)A^4 - \tfrac{12}{16}\varepsilon_1\varepsilon_2A^6)$$

$$+ (A^2 + \tfrac{3}{2}\varepsilon_2A^4 + \tfrac{9}{16}\varepsilon_2^2A^6) = P^2. \tag{B4}$$

Equation (B4) can be written in the form

$$\Omega^2 = R_1 \pm \sqrt{R_1^2 - R_2}, \tag{B5}$$

where

$$R_1 = -(\delta^2 - \tfrac{3}{2}\varepsilon_2A^2 - \tfrac{3}{4}\varepsilon_1\varepsilon_2A^4 - 2 - \varepsilon_1A^2)\Big/\left(2 + 2\varepsilon_1A^2 + \frac{\varepsilon_1^2A^4}{2}\right), \tag{B6}$$

$$R_2 = \left(\frac{9}{16}\varepsilon_2^2A^4 + \tfrac{3}{2}\varepsilon_2A^2 + 1 - \frac{P^2}{A^2}\right)\Big/\left(1 + \varepsilon_1A^2 + \frac{\varepsilon_1^2A^4}{4}\right). \tag{B7}$$

Equation (B5) yields two real solutions for Ω provided that the radical term is real and less than R_1; a single real solution is obtained when the radical term is zero or greater than R_1, and no real solution exists when $R_1^2 - R_2 < 0$.

B.2. TWO-TERM HARMONIC SOLUTION (2THB)

In order to improve the accuracy of the SHB approximation one includes higher harmonics in the assumed solution in equation (B1). In this work, only one more term is added to this equation, whereby the two-term approximation, having the same period as the excitation, to the steady state solution of the system in equation (2) with odd non-linearities takes the form

$$u(T) = A_1\cos T + A_3\cos 3T + B_3\sin 3T. \tag{B8}$$

Substituting equation (B8) and its derivatives into equation (2) and using the same procedure followed previously and neglecting the higher order harmonics, one obtains the following coupled non-linear algebraic equations for A_1, A_3, B_3 and the phase ϕ:

$$\tfrac{3}{4}\varepsilon_2A_1^3 + \tfrac{3}{4}\varepsilon_2A_1^2A_3 + \tfrac{3}{2}\varepsilon_2A_1A_3^2 + \tfrac{3}{2}\varepsilon_2A_1B_3^2 + A - A\,\Omega^2 - \frac{\varepsilon_1}{2}\Omega^2A^3$$

$$- \tfrac{3}{2}\varepsilon_1\Omega^2A_1^2A_3 - 5\varepsilon_1\Omega^2A_1^2A_3 - 5\varepsilon_1\Omega^2A_1^2B_3 = P\cos\phi, \tag{B9}$$

$$\tfrac{3}{4}\varepsilon_2A_1^2B_3 - \Omega\delta\,A_1 - \tfrac{3}{2}\varepsilon_1\,\Omega^2\,A_1^2\,B_3 = -P\sin\phi, \tag{B10}$$

$$\tfrac{3}{2}\varepsilon_2A_1^2B_3 + \tfrac{3}{4}\varepsilon_2A_3^2B_3 + \tfrac{3}{4}\varepsilon_2B_3^3 + B_3 - 3A_3\delta\Omega - 9\Omega^2B_3$$

$$- 5\,\varepsilon_1\Omega^2A_1^2B_3 - \tfrac{9}{2}\varepsilon_1\Omega^2A_3^2B_3 - \tfrac{9}{2}\varepsilon_1\Omega^2B_3^3 = 0, \tag{B11}$$

$$\frac{\varepsilon_2}{4}A_1^3 + \tfrac{3}{2}\varepsilon_2 A_1^3 A_3 + \tfrac{3}{4}\varepsilon_2 A_3^2 + \tfrac{3}{4}\varepsilon_2 A_3 B_3^2 + A_3 + 3B_3\delta\Omega - 9A_3\Omega^2$$

$$-\frac{\varepsilon_1}{2}\Omega^2 A_1^3 - 5\varepsilon_1\Omega^2 A_1^2 A_3 - \tfrac{9}{2}\varepsilon_1\Omega^2 A_3^2 - \tfrac{9}{2}\varepsilon_1\Omega^2 A_3 B_3^2 = 0. \tag{B12}$$

These equations may be expressed in a more convenient form as follows. First, squaring and adding equations (B9) and (B10) and solving for Ω^2 leads to

$$a\Omega^4 + b\Omega^2 + c = 0, \tag{B13}$$

where

$$\begin{aligned}
a &= 1 + A_1^2\varepsilon_1 + 3\varepsilon_1 A_1 A_3 + 10\varepsilon_1 A_3^2 + 10\varepsilon_1 B_3^2 + \tfrac{1}{4}\varepsilon_1 A_1^4 + \tfrac{3}{2}\varepsilon_1^2 A_1^3 A_3 + \tfrac{29}{4}\varepsilon_1^2 A_1^2 A_3^2 \\
&\quad + 15\varepsilon_1^2 A_1 A_3^2 + 25\varepsilon_1^2 A_3^4 + \tfrac{29}{4}\varepsilon_1^2 A_1^2 B_3^2 + 15\varepsilon_1^2 A_1 A_3 B_3^2 + 50\varepsilon_1^2 A_3^2 B_3^2 + 25\varepsilon_1^2 B_3^4, \\
b &= \delta^2 - \tfrac{3}{2}\varepsilon_2 A_1^2 - \tfrac{3}{2}\varepsilon_2 A_1 A_3 - 3\varepsilon_2 A_3^2 - 3\varepsilon_2 B_3^2 - \tfrac{3}{4}\varepsilon_1\varepsilon_2 A_1^4 - 3\varepsilon_1\varepsilon_2 A_1^3 A_3 - \tfrac{45}{4}\varepsilon_1\varepsilon_2 A_1^2 A_3^2 \\
&\quad - 12\varepsilon_1\varepsilon_2 A_1 A_3^2 - 15\varepsilon_1\varepsilon_2 A_3^4 - \tfrac{45}{4}\varepsilon_1\varepsilon_2 A_1^2 B_3^2 - 12\varepsilon_1\varepsilon_2 A_1 A_3 B_3^2 - 30\varepsilon_1\varepsilon_2 A_3^2 B_3^2 - 15\varepsilon_1\varepsilon_2 B_3^4 \\
&\quad - 2 - \varepsilon_1 A_1^2 - 3\varepsilon_1 A_1 A_3 - 10\varepsilon_1 A_3^2 - 10\varepsilon_1 B_3^2, \\
c &= \tfrac{9}{16}\varepsilon_2^2 A_1^4 + \tfrac{9}{8}\varepsilon_2^2 A_1^3 A_3 + \tfrac{45}{16}\varepsilon_2^2 A_1^2 A_3^2 + \tfrac{9}{4}\varepsilon_2^2 A_1 A_3^3 + \tfrac{9}{4}\varepsilon_2^2 A_3^4 + \tfrac{45}{16}\varepsilon_2^2 A_1^2 B_3^2 + \tfrac{9}{4}\varepsilon_2^2 A_1 A_3 B_3^2 \\
&\quad + \tfrac{9}{2}\varepsilon_2^2 A_3^2 B_3^2 + \tfrac{9}{4}\varepsilon_2^2 B_3^4 + \tfrac{3}{2}\varepsilon_2 A_1^2 + \tfrac{3}{2}\varepsilon_2 A_1 A_3 + 3\varepsilon_3 A_3^2 + 3\varepsilon_2 B_3^2 + 1 + 3\varepsilon_1\delta\Omega^3 A_1 B_3 \\
&\quad - \tfrac{3}{2}\varepsilon_2\delta\Omega A_1 B_3 - \frac{P^2}{A_1^2}.
\end{aligned} \tag{B14}$$

Next, equations (B11) and (B12) are solved implicitly for A_3 and B_3 respectively:

$$B_3 = \frac{[-\tfrac{3}{4}\varepsilon_2 B_3(A_3^2 + B_3^2) + \tfrac{9}{2}\varepsilon_1\Omega^2 B_3(A_3^2 + B_3^2) + 3A_3\delta\Omega]}{[\tfrac{3}{2}\varepsilon_2 A_1^2 + (1 - 9\Omega^2 - 5\varepsilon_1\Omega^2 A_1^2)]}, \tag{B15}$$

$$A_3 = \frac{\left[A_1^3\left(\frac{\varepsilon_1}{2}\Omega^2 - \frac{\varepsilon_2}{4}\right) - \tfrac{3}{4}\varepsilon_2 A_3(A_3^2 + B_3^2) - 3\delta\Omega B_3 + \tfrac{9}{2}\varepsilon_1\Omega^2 A_3(A_3^2 + B_3^2)\right]}{[\tfrac{3}{2}\varepsilon_2 A_1^2 + 1 - 9\Omega^2 - 5\varepsilon_1\Omega^2 A_1^2]}. \tag{B16}$$

Equation (B13) can be written in the form

$$\Omega^2 = R_3 \pm \sqrt{R_3^2 - R_4}, \tag{B17}$$

where R_3 and R_4 can be calculated from equation (B14) so that $R_3 = (-b/2a)$ and $R_3 = (c/a)$. Equation (B17) has two real solutions provided that $R_3^2 > R_4$ and $\sqrt{R_3^2 - R_4} < R_3$. A single real solution exists provided that $R_3^2 > R_4$ and $\sqrt{R_3^2 - R_4} > R_3$, and no real solution exists when $R_3^2 < R_4$. Equations (B17), (B15) and (B16) were solved iteratively with an accuracy of 10^{-8} to define the steady state solution [21, 27].

APPENDIX C: STABILITY ANALYSIS USING SINGLE TERM ONLY

The stability analysis of the approximate harmonic balance solution in equation (B1) can be carried out by introducing a small perturbation $v(T)$ to the assumed solution (B1): i.e., by

substituting

$$u(T) = A\cos T + v(T) \tag{C1}$$

into equation (B1). This leads to the following non-linear variational equation:

$$\begin{aligned}
&\ddot{v}\Omega^2\left(1 + \varepsilon_1\frac{A^2}{2} + \varepsilon_1 v^2 + 2\varepsilon_1 v A\cos T + \varepsilon_1\frac{A^2}{2}\cos 2T\right)\\
&\quad + \dot{v}(\delta\Omega - 2\varepsilon_1\Omega^2 A v\sin T - \varepsilon_1\Omega^2 A^2\sin 2T)\\
&\quad + v\left(\tfrac{3}{2}\varepsilon_2 A^2 + 1 - \varepsilon_1\Omega^2\frac{A^2}{2} + \varepsilon_1\Omega^2\dot{v}^2 + \tfrac{3}{2}\varepsilon_2 A^2\cos 2T - \tfrac{3}{2}\varepsilon_1\Omega^2 A^2\cos 2T\right)\\
&\quad + \varepsilon_1\Omega^2 A^2\dot{v}^2\cos T + v^2 A\cos T(3\varepsilon_2 - \varepsilon_1\Omega^2) + \varepsilon_2 v^3 = \frac{A^2}{4}(2\varepsilon_1\Omega^2 - \varepsilon_2)\cos 3T.
\end{aligned} \tag{C2}$$

The stability is governed by the linearized version of equation (C2). In addition, the excitation term on the right-handside is deleted, because it has no influence on the stability; this leads to the following Hill-type equation;

$$\begin{aligned}
&\ddot{v}\,\Omega^2\left(1 + \varepsilon_1\frac{A^2}{2}(1 + \cos 2T)\right) + \dot{v}(\delta\Omega - \varepsilon_1\Omega^2 A^2\sin 2T)\\
&\quad + v\left(1 + \frac{A^2}{2}(3\varepsilon_2 - \varepsilon_1\Omega^2) + \tfrac{3}{2}A^2\cos 2T(\varepsilon_2 - \varepsilon_1\Omega^2)\right) = 0.
\end{aligned} \tag{C3}$$

Then by virtue of the Floquet theory, a particular solution of the linearized variational equation LVE (C3) is sought in the form [2]

$$v(T) = \mathrm{e}^{\beta T}\eta(T), \tag{C4}$$

where β is defined as the characteristic exponent and $\eta(T)$ is a periodic function with periods T and $T/2$. The solution of $v(T)$ is stable (respectively, unstable) if the real part of β is negative (positive), and the real part of β is zero on the boundary between stable and stable regions [11].

To determine the boundaries of the first unstable region "i.e., analysis I" according to the above procedure described in section 3, one may substitute as a first approximation

$$\eta_1(T) = v(T)_{\beta=0} = b_{1c}\cos(T) + b_{1s}\sin(T) \tag{C5}$$

into equation (C3) and apply the harmonic balance method to obtain a set of the following algebraic equations for (b_{1c}, b_{1s}):

$$\begin{bmatrix} 1 - \Omega^2 + \dfrac{A^2}{4}(3\varepsilon_2 - 2\varepsilon_1\Omega^2) & -\delta\Omega \\ \delta\Omega & 1 - \Omega^2 + \dfrac{A^2}{4}(9\varepsilon_2 - 6\varepsilon_1\Omega^2) \end{bmatrix}\begin{Bmatrix} b_{1c} \\ b_{1s} \end{Bmatrix} = \begin{Bmatrix} 0 \\ 0 \end{Bmatrix}. \tag{C6}$$

Non-trivial solutions for b_{1c}, b_{1s} exist only when the determinant of the coefficient matrix in equation (C9) vanishes, which gives the relation

$$\Omega^4(1+2\varepsilon_1 A^2+\tfrac{3}{4}\varepsilon_1^2 A^4)+\Omega^2(\delta^2-2-A^2(3\varepsilon_2+2\varepsilon_1)-\tfrac{9}{4}\varepsilon_1\varepsilon_2 A^4)+(1+3\varepsilon_2 A^2+\tfrac{27}{16}\varepsilon_2^2 A^4)=0. \tag{C7}$$

Solving this last equation for Ω^2 gives the boundaries of the first order unstable region. The boundaries of the second unstable region "i.e., analysis II", which may give rise to the period-doubling bifurcation (PDB), can be obtained by substituting the following equation as a first approximation

$$\eta_{\mathrm{II}}(T) = v(T)_{\beta=0} = b_0 + b_{2c}\cos(2T) + b_{2s}\sin(2T) \tag{C8}$$

into equation (C3) and applying the harmonic balance method to obtain the set of algebraic equations

$$\begin{bmatrix} 1+\dfrac{A^2}{2}(3\varepsilon_2-\varepsilon_1\Omega^2) & 0 & \dfrac{3A^2}{4}(\varepsilon_2-\varepsilon_1\Omega^2) \\ 0 & 1-4\Omega^2+\dfrac{A^2}{2}(3\varepsilon_2-5\varepsilon_1\Omega^2) & -2\delta\Omega \\ \dfrac{3A^2}{2}(\varepsilon_2-\varepsilon_1\Omega^2) & 2\delta\Omega & 1-4\Omega^2+\dfrac{A^2}{2}(3\varepsilon_2-5\varepsilon_1\Omega^2) \end{bmatrix} \times \begin{Bmatrix} b_0 \\ b_{2s} \\ b_{2c} \end{Bmatrix} = \begin{Bmatrix} 0 \\ 0 \\ 0 \end{Bmatrix}. \tag{C9}$$

Non-trival solutions for b_0, b_{2s}, b_{2c} exist only when the determinant of the coefficient matrix in equation (C9) vanishes, which gives the following relation between A and Ω, for certain system parameters δ, ε_1, ε_2:

$$\begin{aligned} &\frac{A^6}{16}(\varepsilon_2^3-99\varepsilon_1\varepsilon_2\Omega^2+93\varepsilon_1^2\varepsilon_2\Omega^4-5\varepsilon_1^3\Omega^6) \\ &+\frac{A^4}{8}(45\varepsilon_2^2-\Omega^2(108\varepsilon_2^2+114\varepsilon_1\varepsilon_2)+\Omega^4(216\varepsilon_1\varepsilon_2+61\varepsilon_1^2)-44\varepsilon_1^2\Omega^6) \\ &+\frac{A^2}{2}(9\varepsilon_2+\Omega^2(12\delta^2\varepsilon_2-48\varepsilon_2-11\varepsilon_1)+\Omega^4(48\varepsilon_1+48\varepsilon_2-4\delta^2\varepsilon_1)-16\varepsilon_1\Omega^6) \\ &+1+\Omega^2(4\delta^2-8)+16\Omega^4=0, \end{aligned} \tag{C10}$$

which is to be satisfied at the stability boundary. Equation (C10) can be solved for A^2 to give the boundaries of the second unstable region and the critical bifurcation value of the amplitude.